ACS Catalysis

Perspective

pubs.acs.org/acscatalysis

Beyond Ordered Materials: Understanding Catalytic Sites on Amorphous Solids

Bryan R. Goldsmith,*[,†,δ] Baron Peters,[‡,§] J. Karl Johnson,[∥] Bruce C. Gates,[⊥] and Susannah L. Scott*[,‡,§]

[†]Fritz-Haber-Institut der Max-Planck-Gesellschaft, Faradayweg 4-6, D-14195 Berlin, Germany

[δ]Department of Chemical Engineering, University of Michigan, Ann Arbor, Michigan 48105, United States

[‡]Department of Chemical Engineering, University of California, Santa Barbara, California 93106, United States

[§]Department of Chemistry & Biochemistry, University of California, Santa Barbara, California 93106, United States

[∥]Department of Chemical and Petroleum Engineering, University of Pittsburgh, Pittsburgh, Pennsylvania 15261, United States

[⊥]Department of Chemical Engineering, University of California, Davis, California 95616, United States

ABSTRACT: Amorphous materials are widely used as components of solid catalysts and have been the subject of much applied research. In some instances, their catalytic performance is demonstrably superior to that of their crystalline counterparts, due in part to their greater flexibility. Amorphous or disordered phases can also be generated from crystalline phases under reaction conditions, and thus, *ex situ* observations of long-range order may provide an incomplete or misleading picture. Until recently, theorists and experimentalists have mostly neglected these important materials in fundamental studies, preferring instead to study "well-defined" (often crystalline) catalysts that are potentially more tractable and amenable to computational modeling of their structure−activity relationships. The amorphous materials were assumed to be simply nonuniform versions of compositionally similar materials with long-range order, having the same key features at short and medium length scales. In this Perspective, shortcomings of this assumption are discussed, as well as challenges inherent in tackling amorphous catalysts more directly, namely, identifying and describing the active sites (especially under reaction conditions), discerning how subtle structural variations modulate site activity, and building atomically detailed models of amorphous catalysts. Three important classes of amorphous catalytic materials are highlighted to illustrate key issues: amorphous oxides, metal ions atomically dispersed on amorphous supports, and supported metal clusters. Amorphous and disordered silicas, aluminas, and silica−aluminas are discussed in terms of challenges and progress toward identifying how their local structural disorder and surface heterogeneity may impact the behavior of active sites. Promising models of amorphous materials with atomistic detail and increased fidelity to experiment are becoming available. However, for reactions in which small fractions of sites dominate the total activity, computational estimates of the observed kinetics will require statistical sampling methods, even for the most detailed catalyst models. Further developments in *in situ* and *operando* characterization techniques and computational modeling will advance our understanding of amorphous catalytic materials and the impact of structural disorder.

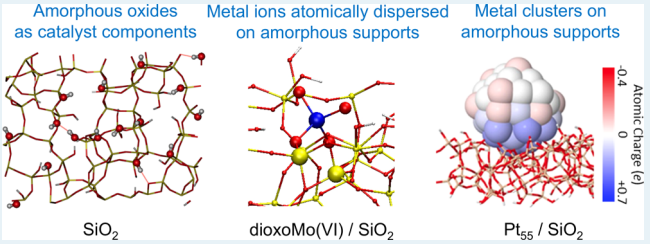

KEYWORDS: *amorphous oxides, supported metal clusters, dispersed metal ions, noncrystalline catalysts, heterogeneity, atomic-level characterization, first-principles modeling*

1. INTRODUCTION

Ever since H. S. Taylor articulated the seminal concept of active sites on catalytic surfaces,[1] including the idea that there is a distribution of such sites with varying reactivity associated with heterogeneity in the local coordination environment, researchers have been attempting to identify and describe them. In the last half-century, many of the seminal advances in our understanding of catalysis have emerged from the study of model catalysts with uniform catalytic sites, including single-crystal surfaces and ordered microporous materials. Recognition of these achievements resulted in a Nobel prize to G. Ertl for understanding chemical processes on solid surfaces via modern surface-science approaches (e.g., CO oxidation on well-ordered platinum surfaces).[2]

Although much insight into catalysis can be gained from studying well-defined model systems, the major components of commercial catalysts are often amorphous (lacking long-range order)[3] rather than crystalline materials, chosen not only because they are typically inexpensive and have highly tunable physical properties such as porosity but also because their activities and productivities can be significantly higher.[4−9]

Received: May 30, 2017
Revised: September 4, 2017
Published: September 13, 2017

DOI: 10.1021/acscatal.7b01767
ACS Catal. 2017, 7, 7543−7557

However, the inherent heterogeneity in both composition and structure of amorphous catalysts makes identification of their active sites extremely challenging. Structures are often sensitive to synthesis conditions and can change under reaction conditions. Furthermore, a small fraction of surface sites may contribute most of the observed reactivity.[8]

Silica is a prototypical amorphous material present in many solid catalysts,[10,11] whereas crystalline silica polymorphs are almost never used, in part because of their much lower surface areas. Amorphous silicas with regular mesopore structures, such as MCM-41 and SBA-15, are valuable as model catalyst supports. Silica–aluminas with high silica contents are also amorphous. Zeolite stabilization through steaming is accompanied by the appearance of extra-framework amorphous silica–alumina.[12,13] Amorphous alumina can also be prepared and is believed to have a greater concentration of defects (e.g., anion vacancies) and more distorted (Lewis acidic) Al sites than its crystalline counterparts.[14−17] Even the transition aluminas such as γ-Al_2O_3, which have powder X-ray diffraction patterns, exhibit various degrees of disorder depending on the synthesis conditions.[18−20] Amorphous mixed-metal oxides like hopcalite (Cu–Mn mixed oxide) are used to catalyze CO oxidation and the decomposition of volatile organic compounds in gas streams.[21,22] The importance of amorphous structures in catalysis is not limited to oxides. For example, amorphous Ni–B and Ni–P alloys show more activity as hydrogenation catalysts than microcrystalline Raney nickel.[23,24] Functionalized amorphous carbon is an active catalyst for biodiesel production, whereas its crystalline forms are inactive.[25] Amorphous metal sulfides and borides are reported to be more active hydrogen evolution electrocatalysts than the corresponding crystalline forms.[7,26]

The evolution of catalysts that are nominally crystalline into amorphous forms in their working state appears to be a common phenomenon. For example, $VOHPO_4{\cdot}0.5H_2O$ catalyzes the selective oxidation of *n*-butane to maleic anhydride and is introduced into the reactor as a crystalline material;[27] however, it is transformed under reaction conditions to a highly disordered phase which is inferred to be the catalytically active phase. Likewise, alkene ammoxidation catalysts (e.g., $Bi_2Mo_xO_y$ and $MoVNbTeO_x$) may be disordered under reaction conditions.[28,29] As another example, an X-ray amorphous $CoO_x(OH)_y$ surface shell that forms reversibly on crystalline Co_3O_4 under electrochemical conditions was found to be essential to its high oxygen evolution activity (Figure 1).[30] Amorphization is accompanied by a partial change in Co coordination from tetrahedral to octahedral and an increase in the average Co oxidation state. Thus, *ex situ* observations of static long-range order may give a misleading picture of these inherently dynamic systems. The structures of well-defined nanomaterials such as crystalline metal particles and ordered metal–organic frameworks often used as precatalysts may bear little resemblance to the active sites of the catalytic materials.[31]

Amorphous oxides (e.g., SiO_2) have often been assumed to have local structures similar to those of compositionally similar crystalline polymorphs, but with very small ordered domains.[32] For example, the surface of amorphous silica has been modeled as a mixture of various crystal terminations of β-cristobalite.[33] However, while these models strictly match the local (i.e., first-coordination sphere) environment of Si, they reproduce neither the siloxane ring-size distribution nor the silanol type distribution of amorphous silicas.[34] Incompletely condensed silsesquioxanes, which are highly convex molecular clusters

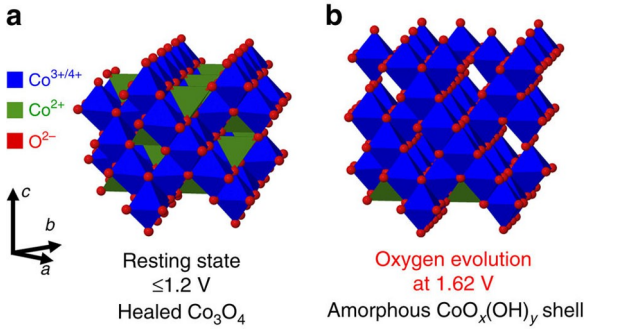

Figure 1. Schematic of possible near-surface structures on a crystalline Co_3O_4 core under electrochemical conditions during the oxygen evolution reaction. (a) At potentials below Co redox features, Co_3O_4 exists in a healed resting state, in which reduced Co sites caused by defects in the near-surface are oxidized to Co_3O_4. (b) At elevated anodic electrode potentials, the Co_3O_4 surface is transformed into $CoO_x(OH)_y$, leading to reversible amorphization of the active subnanometer-thick shell. This $CoO_x(OH)_y$ shell consists of di-μ-oxo-bridged $Co^{3+/4+}$ ions with random site occupancy in the ideal cubic close-packed O^{2-} lattice. Adapted with permission from ref 30. Copyright 2015 Nature Publishing Group.

decorated with silanols, have been used (with limited success) as molecular models for silica on the basis of a geometric resemblance between their silanol arrangement and the ordered hydroxyls on the (111) surface of β-cristobalite.[35−38] However, the reactivity of incompletely condensed silsequioxanes often bears little resemblance to that of amorphous silica,[35,39] and their tendency to form oligomeric complexes in solution hinders their value as models for isolated catalyst sites.[40] An additional important issue for amorphous aluminas is the greater variability in local Al coordination environments (number and geometric arrangement of oxygen ions), relative to those found in crystalline aluminas.

Recent developments in both experimental capabilities and theory promise long-awaited progress in our understanding of heterogeneous materials; thus, it is timely that more attention is now focused on the investigation of amorphous catalysts.[41] Expanding our fundamental knowledge about the important roles of heterogeneity, disorder, and dynamic catalyst behavior will advance catalysis science beyond the study of ideal systems to approach the complexity of real working catalysts.

For this Perspective, we selected the three classes of catalysts shown in Figure 2 to illustrate key issues in understanding and describing heterogeneity: (a) amorphous oxides, (b) metal ions atomically dispersed on amorphous supports, and (c) metal clusters interacting with amorphous supports. First, we discuss experimental and computational investigations of amorphous catalytic materials, focusing on the characterization of surface heterogeneity and the nature of the active sites. Note, we focus primarily on simple oxide supports such as silica and alumina; more complicated oxides such as amorphous mixed cobalt oxide/phosphate are beyond the scope of this Perspective.[42] Next, various *ab initio* modeling approaches are assessed, particularly regarding the challenges posed by amorphous materials. The importance of statistical considerations in the interpretation of activity predictions is also emphasized. Opportunities for collaborations between theorists and experimentalists to improve our understanding of amorphous catalysts are highlighted, especially in the development of more realistic structural models for amorphous catalysts, and the

DOI: 10.1021/acscatal.7b01767
ACS Catal. 2017, 7, 7543−7557

atomic-level characterization of their surface sites in reactive environments.

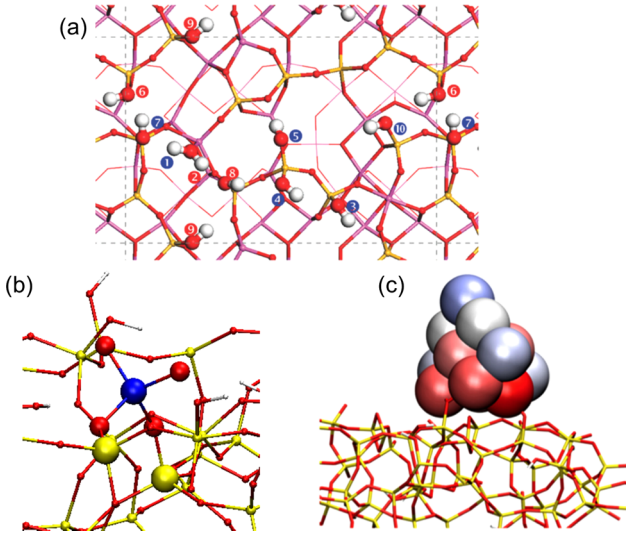

Figure 2. Illustrative examples of three important classes of amorphous catalytic materials: (a) *Amorphous oxides:* Silica–alumina, represented by a slab model with various exposed hydroxyl groups and embedded aluminum centers (O = red; Al = pink; Si = yellow; H = white). Numbers denote distinct types of Brønsted acid sites. Red labels indicate sites capable of protonating lutidine). (b) *Metal ions atomically dispersed on amorphous supports:* A slab model for an isolated dioxoMo(VI) site covalently attached to amorphous silica, generated by DFT geometry optimization (O = red; Mo = blue; Si = yellow; H = white). (c) *Supported metal clusters:* Model of a Pt_{13} cluster interacting with amorphous silica, showing the charge depletion experienced by interfacial Pt atoms (red) interacting with surface hydroxyl groups, and their electron-rich Pt neighbors (blue). Gray-colored Pt atoms are approximately neutral. Figure 2a is from ref 43, with permission from The Royal Society of Chemistry, Copyright 2012; Figure 2c is adapted from ref 44, with permission from the American Chemical Society, Copyright 2015.

2. EXPERIMENTAL AND COMPUTATIONAL APPROACHES IN THE INVESTIGATION OF AMORPHOUS CATALYSTS

2.1. Amorphous Oxides as Catalysts and Catalyst Supports. Amorphous and disordered silicas, aluminas, and silica–aluminas are all common catalyst components because (1) many of them are mechanically and thermally robust, with high surface areas associated with interconnected micro- and mesopores to allow for relatively rapid mass transport of reactants and products, and (2) they can impart stability and activity to a wide variety of catalytically active phases dispersed on their surfaces.[45,46] Powders and pellets of these partially or completely amorphous oxides, often consisting of microparticle aggregates held together by interparticle interactions, are widely used in industrial catalytic processes.

Amorphous silica is used as the support for catalysts in the industrial production of sulfuric acid, 1-alkenes, and polyethene.[47] Silica is relatively simple and chemically inert in comparison to other common oxides, having limited neutral and positively charged oxygen vacancies at most operating temperatures,[48] and almost no redox chemistry. Tremendous effort has been expended over many decades in characterizing its bulk and surface structure using spectroscopic and scattering techniques (e.g., IR, Raman, solid-state NMR, and inelastic neutron scattering).[49−51] Yet, the influence of structural disorder and surface heterogeneity of amorphous silica on the behavior of active sites remains difficult to probe and is still poorly understood.

While both amorphous and crystalline silicas have very high short-range order (all Si atoms are tetrahedral, with four oxygen ligands, in both types of material), amorphous silica has no long-range order, and limited medium-range order. The bulk structure of amorphous silica is believed to be based on the organization of corner-sharing $[SiO_4]^{4-}$ units randomly into siloxane rings of various size and strain.[49] Recently, the atomic-level structure of an amorphous silica bilayer grown on Ru(0001) was resolved in real space (Figure 3).[52,53] This system offers exciting opportunities to probe its structure–reactivity relationships. The silica bilayer is amorphous in the *xy*-plane (substrate plane), although it is ordered in the *z*-direction and atomically flat at the surface. Based on a statistical analysis, a log-normal ring size distribution centered on six as the most abundant ring size (i.e., Si_6O_6) was observed across the silica bilayer, Figure 3b.[52,54] Formation energy calculations for the various-sized silica rings using density-functional theory (DFT) correlate with the population of ring sizes as determined by STM, as does a theoretical silica model constructed using random network theory.[52,54−56] Combinations of ring sizes that share a common Si atom (ring triplets *klm*, with ring sizes of *k*, *l*, and *m*) were examined to search for short-range correlations. The most common ring triplets were 567, 667, and 566, which were inferred to be most probable due to strain minimization.[54] It has been demonstrated experimentally[57] and computationally[9,58,59] that local strain in silica rings can have a large effect on catalyst formation and activity.

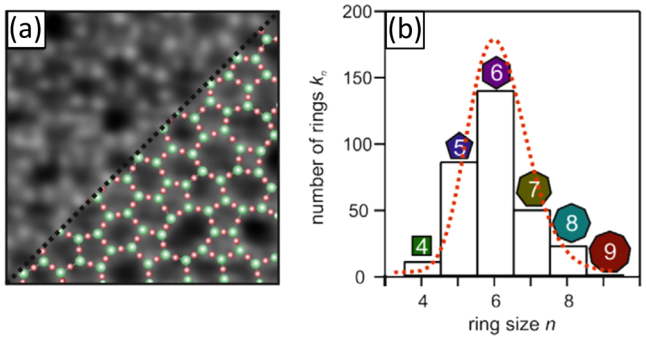

Figure 3. (a) Atomic-resolution STM image of an amorphous silica bilayer on Ru(0001). Silicon atoms appear at the center of SiO_3 triangles that correspond to SiO_4 tetrahedra in three dimensions. In the lower right corner of the image, atomic positions are denoted with green (Si) and red (O) spheres. (b) Ring size distribution of the amorphous silica bilayer determined by STM (histogram of 317 rings, partially displayed in Figure 3a). The red dashed curve is a log-normal fit. Adapted from ref 54, with permission from Elsevier, Copyright 2016.

Much of the chemistry associated with amorphous silicas is controlled by their surface hydroxyl groups. As synthesized, the silica bilayers described above lack such hydroxyls. Recently, however, silanols were generated in one of these films by depositing an amorphous layer of solid water, then irradiating the surface with a low-energy electron beam.[60] Future work on adsorbing various catalyst components onto hydroxylated amorphous silica films may allow these materials to serve as

DOI: 10.1021/acscatal.7b01767
ACS Catal. 2017, 7, 7543−7557

interesting structural models for silica-based catalysts, although the proximity of the catalytic sites to the underlying metal surface creates opportunities for undesired side-reactions.

Transition aluminas are used as catalysts for a variety of industrial reactions including H_2S decomposition (the Claus process), alcohol dehydration, and alkene isomerization.[18] They are also used as catalyst supports in petroleum naphtha reforming and oil hydroprocessing, as well as in many selective hydrocarbon oxidation reactions.[61,62] The surface chemistry of the transition aluminas, exemplified by the high surface area polymorph γ-Al_2O_3, has been reviewed recently.[18] Amorphous forms differ from the transition aluminas in their hydroxyl populations, as well as in their Lewis acidities.[63−67] Multiple alumina phases are sometimes present and may be interconverted during catalyst preparation and use. Computational models of the transition and amorphous alumina surfaces, incorporating both acidic (bridging) and basic (terminal) hydroxyl groups and three-, four-, and five-coordinate Lewis acidic Al^{3+} sites, have improved over the years,[19,68−71] but their relationships to the real materials continue to be debated.

Amorphous silica−alumina is a common support (or support component) for catalysts used in hydrocarbon cracking and is considered promising as a component of biomass conversion catalysts, due to its greater hydrothermal stability compared to either silica or alumina alone.[61,72] The structure and surface chemistry of amorphous silica−alumina have been the subjects of many spectroscopic and computational investigations.[73−76] It is often denoted SiO_2−Al_2O_3, although silica-rich forms are mixed oxides rather than a mixture of oxides, with isomorphic Al^{3+} substitution for Si^{4+} ions. Interestingly, their surface chemistry differs significantly from those of the crystalline aluminosilicates (e.g., zeolites). Unlike zeolites, silica−aluminas possess significant Lewis acidity. Their Brønsted acidity, while stronger than those of silica or alumina, is weaker than that of zeolites, which makes them particularly useful in selective hydrocracking reactions. The lower cracking activity of amorphous silica−aluminas relative to the zeolite mordenite was deemed to result from their preference for alkoxide reaction pathways, due to their limited ability to stabilize carbocations.[77]

The origin of the strong Brønsted and Lewis acidity of amorphous silica−aluminas has been a topic of sustained research interest. Four-, five-, and six-coordinate Lewis acidic Al^{3+} sites have been proposed to be present based on interpretation of spectral data.[74] Typically, the only hydroxyl groups detected spectroscopically on dehydrated SiO_2−Al_2O_3 are terminal silanols.[74,78] Zeolite-like bridging hydroxyl groups are sometimes proposed to be present, but may be associated with samples compromised by traces of adventitious water, which is difficult to exclude from dehydrated amorphous silica−aluminas because they are extremely hygroscopic.[79−82] The high Brønsted acid strength of amorphous silica−alumina compared with that of SiO_2 and Al_2O_3 may arise from the stabilization of deprotonated silanolate groups by their interaction with a nearby coordinatively unsaturated Lewis acidic Al^{3+} site, Figure 4b (in contrast to that of zeolites, which have a high Brønsted acid strength as a result of the presence of bridging hydroxyl groups, Figure 4a).[74,78] Coordination of the silanolate to aluminum upon deprotonation, possibly involving displacement of another siloxane interacting with aluminum, requires considerable framework flexibility which should be much more accessible in amorphous silica−aluminas relative to crystalline aluminosilicates.

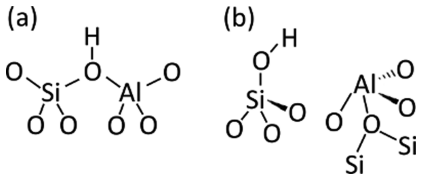

Figure 4. (a) The bridging hydroxyl group (Si-(OH)-Al) is responsible for the strong Brønsted acidity of zeolites. (b) The high Brønsted acid strength of silica−aluminas is suggested to arise when terminal Si−OH groups are located near tetrahedrally coordinatively Al^{3+} sites, which stabilize the corresponding silanolate anions. Upon coordination with the silanolate anion the flexible siloxane ligand may be displaced from Al^{3+}, thereby retaining its tetrahedral coordination.

2.2. Metal Ions Atomically Dispersed on Amorphous Supports. A few examples of important catalysts that involve isolated metal ions dispersed on high surface area amorphous or disordered supports include CrO_x/SiO_2, MoO_x/Al_2O_3, WO_x/SiO_2, and ReO_x/Al_2O_3.[6,47,83−86] They have long been used for the industrial production of polyolefins and in large-scale, continuous alkene metathesis. The catalysts are prepared as highly dispersed metal cations, which have much higher activities than their aggregated metal oxide counterparts.

Isolated metal ions on amorphous supports can also be synthesized by reactions of mononuclear precursor complexes with the functional groups that exist naturally on the support or that are installed by prior surface modification.[87] Catalysts made in this way usually consist of a well-defined component (i.e., the metal ion and its residual molecular ligands) and an amorphous component (i.e., ligands that are part of the support), Figure 5. Subtle structural variations in such active sites dispersed on silica can include Si−O−M bond angles, metallasiloxane ring strain, and variable coordination of siloxane donor ligands.[57,59,88] This is a crucial point, since the nonuniformity of the amorphous component complicates efforts to elucidate catalyst structures and reaction mechanisms and to construct meaningful structure−catalytic activity relationships.

In the case of supported CrO_x catalysts for ethene polymerization (commonly known as Phillips catalysts), structural heterogeneity in the support and the support composition are expected to cause substantial variation in the relative rates of initiation, propagation, and termination

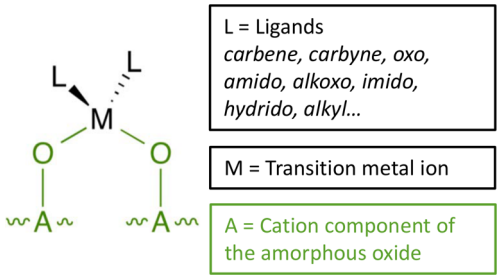

Figure 5. Schematic of an isolated metal ion M^{n+}, with molecular ligands L derived from a precursor metal complex, attached via surface oxygen ligands to an amorphous oxide support with cations A^{m+}. Adapted from ref 8, with permission from AIP Publishing, Copyright 2015.

DOI: 10.1021/acscatal.7b01767
ACS Catal. 2017, 7, 7543−7557

steps.[59,89−91] For instance, the presence of Ti^{4+} ions in the silica support accelerates the initiation process, while the addition of Al^{3+} ions to the silica support increases the sensitivity of the active sites toward H_2 as a chain transfer agent. However, the use of a crystalline support in CrO_x/Al_2O_3 gives only about 10−20% of the polymerization activity of the fully amorphous CrO_x/SiO_2; TiO_2 is also a poor support for chromium oxide.[6] The important influence of variable CrO_x/SiO_2 catalyst site environments is consistent with the known propensity of the catalyst to produce polyethene with high dispersities (typically, 20−30), its ability to coproduce 1-alkenes and to incorporate them as short-chain branches, and to reincorporate terminated chains as long-chain branches. Since each of these features likely requires a slightly different active site configuration, "single-site" models of catalysts such as CrO_x/SiO_2 are understandably inadequate to describe their catalytic behavior in detail.

Indeed, although CrO_x/SiO_2 has been used successfully for more than six decades in the industrial production of high-density polyethene, the mechanism by which the inorganic precursor sites of this catalyst spontaneously initiate polymerization remains hotly disputed,[89,90,92−95] even though the chain propagation mechanism has been settled for some time. Experiments, DFT calculations and microkinetic modeling have repeatedly suggested that Cossee−Arlman propagation at a monoalkylchromium(III) site is the most likely ethene polymerization mechanism.[89] Recent DFT calculations using cluster models by some of the authors suggested that the initial activation of Cr(II) sites to yield monoalkylchromium(III) sites could occur by oxidative disproportionation of ethene followed by homolytic Cr−C bond cleavage,[96] which is supported by the *in situ* experimental observation of vinyl sites $(\equiv SiO)_2Cr^{III}-CH=CH_2$, an electron paramagnetic resonance signal characteristic of organic radicals, and GC detection of *n*-butane.[97−99] Based on the computational evidence, this mechanism appears to require hemilability of the spectator siloxane ligands to facilitate the homolysis step while still enabling ethene oxidative addition, Figure 6.[96] Reactions requiring hemilabile spectator ligands could be promoted by the greater flexibility of amorphous silicas, compared with their crystalline counterparts.

Recently, initiation of the Phillips catalyst by heterolytic C−H bond activation[100] of ethene was examined with DFT calculations for five different $(SiO)_3Cr(III)$ sites on an amorphous silica slab model.[91] One of the five sites was viable for all of the required steps (initiation, polymer chain growth, and termination without deactivation). In this sense, the authors addressed an earlier critique of this mechanism by Peters et al.[92] They also demonstrated that different sites can differ in reaction energy by as much as 150 kJ/mol for the same elementary step. However, the proposed $(SiO)_3Cr(III)$ sites were created by artificially changing entire ≡SiOH groups in the amorphous silica model into Cr ions, and in the process generating highly strained environments that may not be accessible via actual chemical grafting or calcination processes. We stress that the thermal energy k_BT at typical calcination temperatures (ca. 10 kJ/mol) is vastly smaller than the free energy differences between these sites (e.g., > 100 kJ/mol for some reactions). Moreover, the alchemical manner in which these sites were created prevents any quantitative assessment of their abundance versus the abundance levels that would explain the observed catalyst activity.[7] For those catalysts having active species that are grafted on the support and activated with no or only mild treatment, questions about site heterogeneity could begin to be addressed more seriously by using atomistically detailed models of the amorphous support and by explicitly modeling the grafting and thermal activation steps.

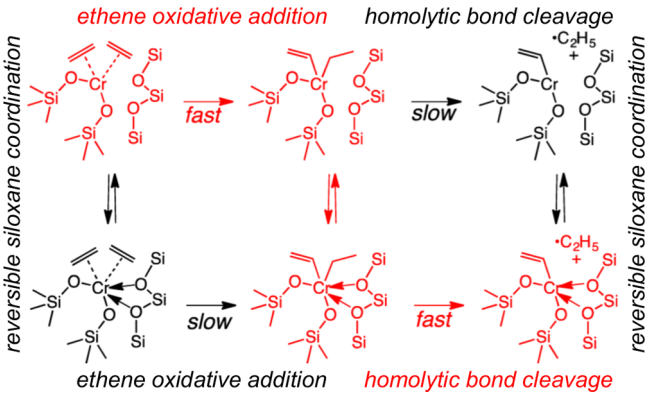

Figure 6. A proposed Phillips catalyst initiation mechanism requiring flexibility in the amorphous silica support. Ethene oxidative addition followed by homolytic bond cleavage on isolated $Cr(II)/SiO_2$ precursor sites yields activated monoalkylchromium(III) sites. The homolysis rate is promoted by the interaction of siloxane ligands with Cr, but ethene oxidative addition is faster when the siloxanes dissociate. Structures in red show a possible path for fast site activation involving reversible coordination of hemilabile siloxane ligands. Adapted from ref 96, with permission from the American Chemical Society, Copyright 2016.

In a second example, supported methyltrioxorhenium (CH_3ReO_3, MTO) has been used as a model for $Re_2O_7/SiO_2-Al_2O_3$ and Re_2O_7/Al_2O_3, which are alkene metathesis catalysts active at room temperature. The initiation of alkene metathesis catalyzed by supported MTO (and similarly, supported Re_2O_7) is still incompletely understood, despite much effort.[101−108] Since solutions of MTO do not catalyze alkene metathesis in the absence of a Lewis acid, the oxide support is inferred to serve as an activator. Metathesis activity correlates with the availability of Lewis acid sites; MTO interacting with Brønsted acid sites was found to be unreactive.[103] Crystalline zeolite Y[109] and γ-alumina[110,111] are much less effective in activating MTO than amorphous silica−alumina,[103] which is in turn less effective than chlorinated (and disordered at the surface) alumina.[107] Some of the proposed structures are shown in Figure 7. The involvement of three-coordinate Al sites has been suggested in promoting the formation of a bridging methylene (**C**) which could be the precursor of an active terminal methylene;[112] however, the most active catalysts lack the ^{13}C NMR signal assigned to this site,[103,107] and three-coordinate Al sites which were proposed computationally[108] have yet to be detected experimentally. Further understanding of how the local environment of the surface aluminum ions, which is related to the Lewis acidity, is needed to advance our understanding of the activation of MTO.

2.3. Metal Clusters Dispersed on Amorphous Supports. Metal and metal oxide clusters (i.e., particles with diameters less than about 10 Å) dispersed on amorphous supports catalyze a broad range of reactions. In this section, we focus primarily on metal clusters dispersed on supports such as silica and alumina. These catalysts are traditionally made by impregnating a porous support with a solution of a metal salt, followed by calcination in air or O_2 and reduction in H_2.[45] However, this procedure usually gives mixtures of clusters of

DOI: 10.1021/acscatal.7b01767
ACS Catal. 2017, 7, 7543−7557

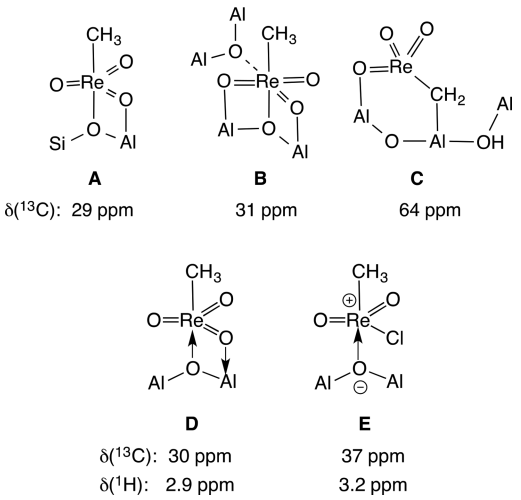

Figure 7. Proposed structures, with observed NMR chemical shifts, for intact MTO grafted onto SiO_2–Al_2O_3 (**A**),[103] and γ-Al_2O_3 (**B**),[106,112] as well as a proposed methylene-bridged structure on γ-Al_2O_3 (**C**).[106,112] Recently, Gallo et al. assigned NMR signals for MTO interacting with unchlorinated (**D**) and chlorinated (**E**) regions of the Cl–Al_2O_3 surface.[107] Naturally, the coordination numbers and geometries of the support Al atoms are variable, leading to considerable heterogeneity in the grafted sites. Adapted from ref 107, with permission from the American Chemical Society, Copyright 2016.

various sizes. In contrast, supported metal clusters made by reaction of a molecular precursor with a support, by a surface-mediated synthesis, or by mass-selection in a molecular beam, are often more uniform, at least initially.[45,113−115] These alternative syntheses have revealed that cluster activities and selectivities can be tuned not only by varying the support type but also by adjusting the cluster size atom by atom.[113,116−120]

A major experimental challenge with metal clusters is controlling their size and shape, as well as retarding deactivation. Cluster morphology can change dynamically under reaction conditions,[121−124] and Ostwald ripening, sintering, or cluster disintegration can lead to large changes in cluster size, selectivity, and activity.[125−127] Isolated metal ions that form under reaction conditions may in some cases be responsible for enhanced catalytic activity or selectivity compared with their metal cluster counterparts. Under reactions conditions these isolated metal ions can be highly mobile on the support.[128−130] Indeed, the importance of dynamics in catalysis, whether to deactivate or to form active sites, is so prevalent that catalysts have been referred to as "living" systems.[131] Many metal clusters exhibit such behavior, interconverting readily between multiple structural isomers.[132−135] It is still unknown how the heterogeneity of amorphous supports influences the distribution of cluster isomers, especially under reaction conditions. Due to the increased flexibility of amorphous supports, they may be able to stabilize different cluster structures than crystalline materials by adjusting atom positions to maximize bonding between the support and the cluster.

Metal carbonyl clusters have been explored as molecular precursors of uniform supported metal clusters,[136,137] via cluster decarbonylation with retention of the metal framework. For example, Ir_4/γ-Al_2O_3 was synthesized by adsorption of $Ir_4(CO)_{12}$ followed by decarbonylation. Adsorption of Ir-$(CO)_2$(acac) (acac = acetylacetonato) on γ-Al_2O_3 followed by reductive carbonylation gave supported $[Ir_6(CO)_{15}]^{2-}$ in high yield. Decarbonylation led to supported Ir_6 clusters.[138] Both Ir_4 and Ir_6 clusters likely form metal hydrides via oxidative addition of surface hydroxyl groups. The metal ions in positive oxidation states are likely localized at the metal–support interface.[44,139] EXAFS can provide some information about the metal–support interface, although the information is averaged over the entire sample. The key result is that the metal–support oxygen distances generally observed on both amorphous and crystalline metal oxide (and zeolite) supports are about 2.1 Å,[140] just as observed for mononuclear metal complexes and consistent with positive oxidation states for the metal ions (whereas much longer distances of 2.5–2.7 Å are typical of zerovalent metal clusters).[141]

Well-defined supported metal clusters have been formed by soft-landing of mass-selected clusters onto planar surfaces.[115,142] For instance, Ag_3 clusters deposited on amorphous alumina in this way were investigated in the selective oxidation of propene to propene oxide.[114] Under reaction conditions, sintering of the Ag_3 clusters gave small aggregates with per-surface-atom turnover rates similar to those of Ag_3 but greater selectivity toward propene oxide (rather than the acrolein side-product). The activation energies were computed by DFT for the formation of both products on different Ag sites.[143] The availability of subsurface oxygen was found to control selectivity. In Ag clusters (ca. 50 atoms), oxygen adatoms stabilized at nanoparticle edges result in a lower energy barrier for acrolein production, whereas larger Ag aggregates (modeled as the surface oxide $Ag_{1.83}O$/Ag(111)) are more selective for propene oxide. The higher diffusion barrier for subsurface oxygen in the larger aggregates limits H-abstraction from the oxametallacycle intermediate. The role of the amorphous alumina support in this process is incompletely understood and requires further examination.

First-principles (*ab initio*) modeling can give insight into metal cluster structures and their properties on amorphous supports. According to recent predictions, monodisperse Pt clusters supported on amorphous silicas with varying degrees of hydroxylation may exhibit nonuniform reactivity because the precise location of the cluster on the surface influences the extent of charge transfer across the metal–support boundary.[44] Nonetheless, computational studies of catalysis under realistic conditions remain difficult, and advances in computational modeling are needed before predictions with chemical accuracy (≤1 kcal/mol) become routine. In the following section, we discuss conventional modeling approaches and promising models of amorphous catalytic materials, as well as challenges regarding their accurate modeling.

3. COMPUTATIONAL MODELS OF AMORPHOUS CATALYTIC MATERIALS

3.1. Modeling Using Predefined Structures. Most computational investigations of solid catalysts have long focused on reactions on the surfaces or in the pores of crystalline metals, metal oxides, and zeolites (and, more recently, metal–organic frameworks). Attempts to model reactions involving amorphous catalytic materials, such as the activation of isolated CrO_x species on silica for ethene polymerization[89,90,144−146] and isolated MoO_x and WO_x sites on silica for alkene metathesis,[147−149] are less common. The greater challenges for the amorphous materials arise due to a lack of information about (1) local environments around the catalytic sites, and (2) subtle structural and electronic variations

DOI: 10.1021/acscatal.7b01767
ACS Catal. 2017, 7, 7543−7557

in the diverse site environments. To model these types of materials, *a priori* decisions must be made about likely structures based on incomplete information.

Computational investigations of amorphous catalysts require the use of either *cluster models* or *slab models*. Slab models are technically periodic (unlike an amorphous solid), but they eliminate the artificial boundaries and capping atoms of cluster models.[150] Cluster models are created by "carving out" a small portion of the bulk material as a model for the active site and its surroundings.[151,152] Examples of (a) a small cluster model, and (b) a slab model, both representing an isolated Mo(VI) site covalently attached to amorphous silica during ethene metathesis, are shown in Figure 8. Relatively small cluster models are more common in this type of *ab initio* computation, because of the computational expense of modeling catalytic cycles in larger systems with high-accuracy methods such as MP2,[153] CCSD(T),[154] the random phase approximation,[155] or DFT with hybrid exchange-correlation functionals.[156,157] For insulating materials, in which the local electronic structure is only slightly perturbed by the bulk material, the cluster modeling approach can be appropriate. Fortunately, many amorphous oxide supports and dispersed metal oxide and metal cluster phases fulfill this criterion.

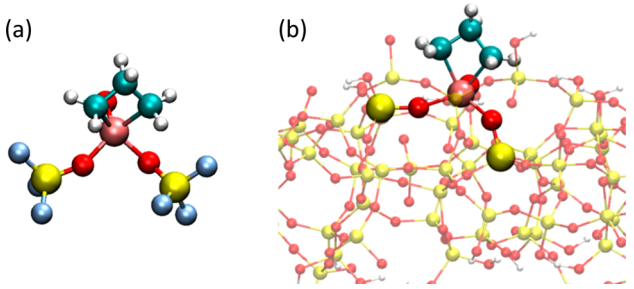

Figure 8. (a) A small cluster model, and (b) a slab model, both representing a molybdenacyclobutane attached to amorphous silica during ethene metathesis. For the cluster model, the positions of the atoms at the periphery (far from the active site) are typically fixed in chemically plausible locations to give the model rigidity and thus solid-like character (O = red; Mo = pink; Si = yellow; H = white; C = teal; F = light blue). Adapted from ref 158, with permission from the American Chemical Society, Copyright 2016.

For cluster models based on crystalline materials such as zeolites, peripheral atoms (i.e., those located at the edge of a cluster model) are usually constrained (fixed) in their crystallographic positions. By contrast, there is no general rule for placement of peripheral atoms in cluster models for amorphous materials. Leaving them unconstrained may make the model too flexible.[103,159] Fixing the peripheral atoms of small clusters results in artificially stiff systems. The locations of the fixed peripheral atoms, as well as the choice of terminating groups, can strongly influence catalyst site properties.[59] Various terminating groups can be selected to mimic the extended structure or to simplify the calculations, with typical choices being OH,[159] F,[89,160] or H.[58] For an oxide support, F is too electronegative, whereas H is too electropositive; OH termination can result in unrealistic hydrogen bonding.

An assumption that is implicit but usually not acknowledged in this approach is that cluster models represent "important" catalyst sites (i.e., those that are sufficiently active and abundant to contribute significantly to the observed activity). For example, incompletely condensed silsesquioxanes with structures based on known homogeneous silica-based compounds are commonly employed cluster models that approximate various hydroxyl terminated sites of amorphous silica (Figure 9).[103,161,162] However, such silsesquioxanes are highly convex, and the siloxane ring size is typically restricted to just eight members (i.e., a 4-ring).[163] The silsesquioxanes are less ideal as model systems of amorphous materials compared to larger cluster models (carved from amorphous slabs) or slab models because of their limited ability to reproduce the structural diversity and reactivity of amorphous systems.

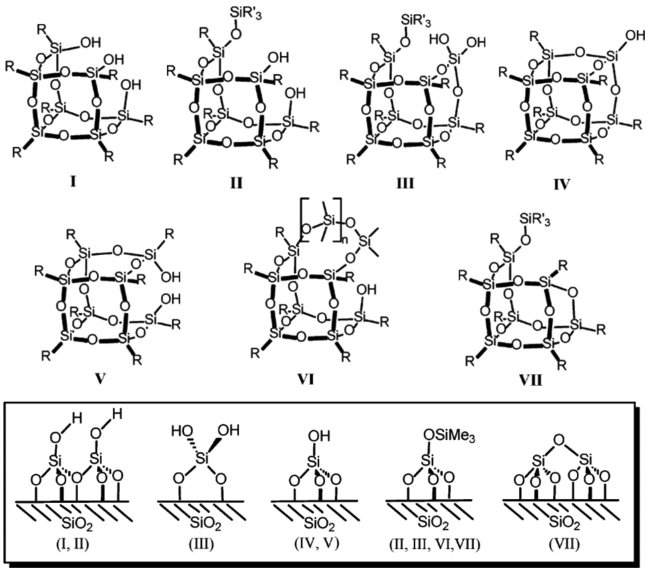

Figure 9. Incompletely condensed silsesquioxanes (upper and middle rows) and the surface silanol and siloxane sites they are intended to model (lower row). We note that vicinal silanol pairs (located on silicon atoms separated by a single siloxane bridge as depicted in the lower left structure) are not generally oriented in a way that allows them to engage in mutual hydrogen bonding,[164] and that the silsesquioxanes I and II do not actually contain vicinal silanols according to this definition. Adapted from ref 163, with permission from the American Chemical Society, Copyright 2002.

Recently, some of us advocated the use of minimal cluster models (i.e., models that make very limited assumptions about the local structure of the catalyst site by including only structural features that can be justified by spectroscopic techniques).[59,165] The idea is that specific structural assumptions required for building large/advanced cluster models could hinder elucidation of general structure−property relationships. Moreover, the results obtained may depend strongly on the structural assumptions of the larger cluster model. Instead, small models may be better at revealing key local structural features that impart heterogeneity to the reactivity of the active sites. However, small cluster models neglect important longer-range structural features present in periodic slab models and hence may not capture all the diversity of an amorphous material.[144,158] Use of several medium-sized cluster models generated from a larger amorphous model may begin to address this limitation;[90,146,166] however, statistical analysis indicates that the number of required models to reliably predict reactivities may be in the thousands (Section 3.3).

Periodic slab models can overcome some of the limitations of finite-sized cluster models.[158] Such slab models naturally incorporate long-range electronic and geometric effects, which

DOI: 10.1021/acscatal.7b01767
ACS Catal. 2017, 7, 7543−7557

can be important for accurate predictions of the bulk and surface properties of many solids. Many studies compare the accuracy of computed energies, vibrational frequencies, and other physicochemical properties obtained from periodic and cluster calculations.[150,167−169] Quantitative results depend on the type and size of the support model, although qualitative trends for periodic slab and cluster models usually remain the same.

Slab models of crystalline materials are routinely used as surrogates for amorphous supports; for example, β-cristobalite is used as a proxy for silica.[170] However, amorphous surface models generated from crystal facets are inadequate to capture the diversity of site environments in amorphous materials. Another approach is to generate amorphous surface models by carving surfaces from melted glasses determined on the basis of molecular dynamics simulations.[171−174] These surfaces contain siloxane rings of varying size, but generating the experimental ring size distribution and silanol type distribution remains a challenge.

Periodic slab models have some drawbacks. Large supercells are required to minimize artificial interactions of adsorbates with their copies in periodic images, and for charged systems sophisticated correction schemes are needed to reach size convergence. To address these issues, aperiodic hybrid quantum mechanical/molecular mechanics (QM/MM) models, whereby a finite QM region is embedded in a surrounding MM environment, could be constructed.[175] ONIOM methods, which are similar to traditional QM/MM approaches, could also be applied to enable studies involving larger system sizes.[176]

3.2. Improving Experimental Fidelity in Computational Models for Amorphous Catalytic Materials. The structure of a material must be known in considerable detail before its properties can be computed. Amorphous catalytic materials are challenging to model due to their lack of symmetry, and because many parameters influence their surface properties (e.g., surface atom coordination number, oxidation state, hydroxyl group type and density, and nanoparticle size and shape). Fortunately, models of amorphous materials and surfaces with atomistic detail and increased fidelity to the actual experimental preparation conditions are becoming available. A stochastic quenching approach initiating from random configurations has been used to model bulk amorphous Al_2O_3,[177] and kinetic Monte Carlo, classical molecular dynamics, and density-functional theory have generated models of MCM-41, an important catalyst support made of amorphous silica with periodic mesopores.[171,178−182] The activated relaxation technique is also efficient for obtaining energy-minimized structures in amorphous materials.[183,184] Reverse Monte Carlo approaches have generated bulk structures for amorphous materials[185] and disordered crystals,[186] although the resulting models can have too much disorder if appropriate structural constraints are not applied (e.g., atom coordination numbers and bond angles).[187]

A promising slab model for amorphous silica−alumina was developed by simulated annealing of a $Si(OH)_4$ film epitaxially deposited on dehydrated γ−Al_2O_3(100).[75,188] It may be more realistic than cluster models of aluminum-substituted silsesquioxanes employed to approximate surface sites in amorphous silica−alumina;[105,189] such models necessarily cannot represent the diversity of site environments present in the material. In the slab model, the surface of amorphous silica−alumina was modeled as a function of water partial pressure and temperature via calculating the adsorption energy of water molecules and using *ab initio* thermodynamics. Various four- and five-coordinate Al^{3+} ions as well as several kinds of hydroxyls were present, enabling a systematic investigation of Lewis and Brønsted acid strengths.[43,76] Interestingly, computed frequency shifts of adsorbed CO did not correlate directly with the Brønsted acidity of various hydroxyl groups in this silica−alumina model,[41] although many experimental studies assume such a relationship. Future studies using this model to examine differences in metal sites interacting with the surface could shed light on the relationship between local heterogeneity in amorphous silica−alumina and the catalytic activity and selectivity of supported metals.

The importance of the type, number, and distribution of hydroxyl groups on oxide surfaces has long been recognized in catalysis. Sustained efforts to understand the properties of surface hydroxyls in amorphous silicas, aluminas, and silica−aluminas have benefited from computational modeling.[171,188,190] For example, a model for the surface of silica was generated by carving a slab from bulk silica followed by capping all dangling bonds with hydroxyl groups.[191] Although the initial version replicated the reported silanol content of fully hydroxylated silica, it did not attempt to predict the temperature dependence of this number. Subsequently, amorphous silica surfaces with various degrees of hydroxylation were developed by inducing incremental condensation of the closest next-neighbor pairs of H-bonded interacting hydroxyl groups.[171]

Developing computational models with hydroxyl populations that evolve with temperature (as they are observed to do experimentally) is still a challenge. Models are needed that reproduce the temperature-dependent abundance of hydrogen-bonded and non-hydrogen-bonded silanols on amorphous silica, as well as the fractions of vicinal pairs, geminal pairs, and isolated silanol groups. In this direction, one of the authors and his colleagues generated amorphous silica slab models with varying surface silanol concentrations using a combination of empirical reactive molecular dynamics, DFT, and *ab initio* thermodynamics.[174] Although this work is a step forward in predicting total silanol numbers, Figure 10 shows that there are still discrepancies between the computed and experimental densities of single (often called isolated) silanols and proximal (often called vicinal) silanols at temperatures below 400 °C.

The silica slab model also fails to predict the decrease in the single (isolated) silanol population at temperatures above 600 °C. A possible explanation is the neglect of proton or silica migration in the model.[192,193] A DFT study of amorphous silica models invoked silica migration (by successive water-assisted rupture and formation of siloxane bridges) at similar temperatures to further decrease the silanol number.[194] However, under many conditions relevant to catalyst preparation (low water vapor pressure in vacuum or in a dry, inert atmosphere), this mechanism may not be the correct explanation, except in the case of the most highly strained rings. If trace water could readily catalyze ring opening of moderately strained or unstrained rings, then the hydroxyl groups on silica would migrate, and condense, at moderate temperatures. However, even when the silica starts to melt at 1200 °C, a significant number of hydroxyl groups persist.[195,196] This strongly suggests that the hydroxyl groups are not mobile and that ring opening/migration is not important at temperatures relevant to catalysis (below 1200 °C). An alternative explanation arises from differences in the assignment of silanol types in experimental

DOI: 10.1021/acscatal.7b01767
ACS Catal. 2017, 7, 7543−7557

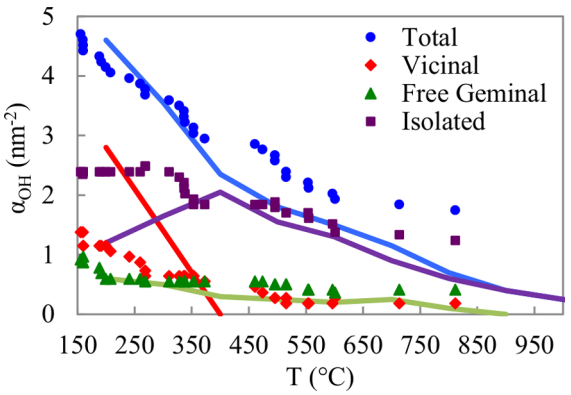

Figure 10. Predicted distribution of silanol groups on amorphous silica as a function of temperature (P_{H_2O} = 10^{-6} bar) from the model of Ewing et al. (points), compared with average reported experimental values (lines). In the original work, silanol types were defined as follows: *vicinal* (meaning proximal) silanols: pairs which exhibit mutual hydrogen bonding, including geminal and nongeminal pairs; *isolated* single silanols, ≡SiOH; *free geminal*: silanediols, ═Si(OH)$_2$ that do not engage in hydrogen-bonding. Adapted from ref 174, with permission from the American Chemical Society, Copyright 2014.

and computational studies. Spectroscopic evidence suggests that many non-hydrogen-bonded silanols are not truly isolated hydroxyl groups, but vicinal silanol pairs (located on silicon atoms separated by a single siloxane bridge) that condense only at temperatures in excess of 600 °C to give highly strained Si_2O_2 rings.[164] In many experimental studies, all non-hydrogen-bonded silanols are designated "isolated", even though neither vicinal nor geminal silanol pairs engage in intrapair hydrogen bonding, and both have O−H stretching frequencies that are indistinguishable from those of truly isolated silanols.[164,197,198] Other experiments have provided evidence for the persistence of a substantial vicinal silanol population even on highly dehydroxylated silicas, via their reaction with $GaMe_3$.[195]

Because of the many types of heterogeneity in local surface structures, modeling support effects requires the time-consuming calculation of a broad distribution of catalyst−support interactions. Recently, a hybrid classical/quantum approach was developed to obtain fast predictions of nanoparticle-amorphous support interactions.[44,199] For Pt nanoparticles on silica, one of the authors reported linear correlations for the particle adhesion energy and net charge as a function of the silanol density, nanoparticle size (Pt_{13}, Pt_{55}, Pt_{140}), and nanoparticle shape.[199] An increase in silica pretreatment temperature weakens nanoparticle adhesion to the surface because fewer Pt−O bonds can be formed to surface silanols. Charge transfer from the Pt nanoparticle to silica is correlated with the number of Pt−O bonds, which cause electron depletion in Pt ions near the interface. Therefore, surface pretreatment temperature can be used to modify the nanoparticle-support interface and thus nanoparticle stability and reactivity, on amorphous silica. Adsorbate binding for such systems is not accurately predicted either by studying nanoparticles in the gas phase or by modeling their interactions with crystalline silica surfaces.

In summary, computational and methodological advances have brought us closer to constructing atomically detailed models of amorphous surfaces, but quantitative accuracy remains elusive because of approximations in underlying electronic-structure theory (or force-field) approaches due to their computational expense (e.g., by using approximate exchange-correlation functionals in density-functional theory applications) and a lack of precise experimental results for comparison.

3.3. Statistical Assessment of Computational Predictions. Since *a priori* knowledge of the activation energy distribution for a heterogeneously catalyzed reaction is usually unavailable, computational investigations must rely on statistical sampling. When the average structural characteristics of multiple, smaller, amorphous silica clusters (72 atoms) were compared with those of larger models (1479 atoms),[166] 10 small cluster models were demonstrated to provide a good statistical sample of structural features consistent with larger simulated glass systems. By extension, we infer that a large number of cluster models will be needed to make predictions about macroscopic reaction rates on amorphous catalysts. Since rates depend exponentially on activation free energies, statistical averaging of results using cluster models will require many more models than does the averaging of structural features, as the following discussion illustrates.

With advances in computing power, the slab model approach seems likely to dominate computational modeling efforts focused on amorphous catalytic materials in the near term, as a consequence of its advantage over cluster modeling in describing flexible extended networks. Nonetheless, slab models still present difficulties for sampling the catalyst activation energy distribution to predict macroscopic rates. The issue has yet to be discussed widely in the catalysis literature. Even the most realistic slab models are still inherently small relative to the length scales of real materials, and consequently may not contain a representative sampling of the active sites. For instance, it is difficult to model a catalyst in which 1% of the potential sites are active when the computational model contains only a few such sites.[8] Unfortunately, sampling the full distribution of active sites will be difficult for some time to come, because: (1) first-principles calculations remain prohibitively expensive to use with Monte Carlo sampling methods, and (2) the active site distribution is unknown and also likely to be non-Boltzmann as a result of its quenched disorder.[8]

Constable hypothesized an exponential distribution of activation energies for a reaction taking place on the nonuniform surface of a catalyst.[200] He further assumed that there is a minimum value for the activation energy, below which no sites exist. The effective value of the activation energy for a particular reaction differs from this minimum value. Recently, some of us presented a statistical framework showing how the distribution of activation energies could in principle be obtained if the distribution of active site structures were known, and how the effective fraction of active sites could be predicted computationally for a given set of reaction conditions.[8] The statistical framework demonstrates that kinetic predictions require information about the low-energy tail of the activation energy distribution, since reactivity is dominated by contributions from the extreme members of the active site distribution. In addition, although the framework assumed a fixed active site distribution invariant to reaction conditions, the distribution could evolve over time and depend on reaction conditions. Ideally, the framework will incorporate time-dependent population balance equations.

Averaging over the activities of all catalyst sites gives the macroscopic rate; however, in both computational and single-molecule spectroscopy studies, the number of catalytic sites sampled is limited. This limitation leads to the following

DOI: 10.1021/acscatal.7b01767
ACS Catal. 2017, 7, 7543−7557

question: when is the number of independent samples of sites N large enough to engender confidence in the predicted rate? A small variance in the activation energy E_a (or the Gibbs activation free energy, within the context of transition state theory) leads to an enormous (relative) variance in reaction rates at individual sites. Even if prefactors are essentially independent of site characteristics, an accurate estimate of the rate requires a sample large enough to accurately estimate $\langle e^{-\beta E_a}\rangle$. Here $\beta = 1/k_B T$ and $\langle ...\rangle$ denotes an average over the ensemble of sites. The central limit theorem (CLT) states that the sample size N should satisfy the following criterion:

$$N + 1 \gg \langle e^{-2\beta E_a}\rangle / \langle e^{-\beta E_a}\rangle^2$$

Note that this version of the CLT inequality has been squared. To ensure that estimates fall within 10% of the actual value of $\langle e^{-2\beta E_a}\rangle$, the number of samples $N + 1$ should be ca. 100 times larger than $\langle e^{-2\beta E_a}\rangle / \langle e^{-\beta E_a}\rangle^2$. Thus, one should determine the size of $\langle e^{-2\beta E_a}\rangle / \langle e^{-\beta E_a}\rangle^2$ to identify an appropriate sample magnitude N. Unfortunately, $\langle e^{-2\beta E_a}\rangle$ is even more difficult to estimate accurately than $\langle e^{-\beta E_a}\rangle$. Instead, the ratio can be approximated using a series of low-order central moments:

$$N + 1 \gg \frac{1 + 2\langle(\delta\beta E_a)^2\rangle - \frac{4}{3}\langle(\delta\beta E_a)^3\rangle + ...}{1 + \langle(\delta\beta E_a)^2\rangle - \frac{1}{3}\langle(\delta\beta E_a)^3\rangle + ...}$$

where $\delta\beta E_a \equiv \beta E_a - \langle\beta E_a\rangle$. Examples in the literature suggest that some activation energy distributions have $\langle(\delta\beta E_a)^2\rangle \gg 1$.[8,59] Therefore, high-order moments will likely be important, and consequently the required value of N may be in the thousands. Clearly, *ab initio* estimates of the observed kinetics, even with the most comprehensive amorphous catalyst models, will require clever sampling methods.

4. OPPORTUNITIES FOR ADVANCES THROUGH JOINT EXPERIMENTAL–COMPUTATIONAL STUDIES

Amorphous catalysts present formidable challenges for active site determination, because their inhomogeneity can be manifested on multiple length scales. Challenges in experimental characterization can be partially alleviated by close interaction with theoretical investigations. This approach has yielded many successes in enhancing understanding of elementary reactions and catalytic processes observed in ultrahigh vacuum surface science experiments. Developments in surface characterization techniques and in computational modeling that are now advancing our understanding of amorphous catalytic materials are discussed in the following sections.

4.1. Developing Improved Models of Amorphous Catalytic Materials. Until recently, efforts to generate computational models of amorphous catalytic materials were often based on questionable approximations; consequently, many predictions were unreliable. Fortunately, advances in electronic-structure theory codes, computing power, simulation methodologies, and experimental characterization techniques are reducing the need for such approximations. For example, improvements in DFT exchange-correlation functionals, which treat the well-known "delocalization" and "static correlation" errors more accurately,[201] are bringing energy predictions closer to chemical accuracy (less than 1 kcal/mol). Methodological developments (e.g., reactive force fields[202] and machine-learned potentials[203−206]) are promising the capability to model amorphous systems with larger sizes and increased complexity. High-throughput calculations and big-data analytics (e.g., compressed sensing, subgroup discovery, and kernel ridge regression) approaches could help researchers discover insights into amorphous catalysts, for instance, by finding geometric and electronic descriptors that predict activity or selectivity,[207−212] facilitating robust curation of large experimental and computational data sets via outlier detection,[213,214] optimizing proposed catalyst reaction networks and quantifying uncertainty,[215] and accelerating the discovery of reaction mechanisms.[216,217] Developments in online materials databases are also playing an important role in catalyst discovery, by enabling data storage for later comparison with other studies as well as for repurposing.[218−221]

Benchmarking theoretical predictions against careful experimental measurements is also essential, because it quickly identifies problems with underlying assumptions and enables the attribution of error bars to predictions.[222] Key metrics for comparison include thermodynamic properties (e.g., reaction enthalpies, reaction entropies, and reaction free energies), kinetic properties (e.g., activation enthalpies, activation entropies, free energy barriers, and macroscopic rate predictions), as well as spectroscopic signals (e.g., IR, NMR, and XAS/XES), Figure 11. Computed reaction pathways should be evaluated for their dependence on local surface heterogeneity. Rate theories such as harmonic transition state theory[223] can be used to predict rate constants and trends in kinetics, thereby allowing evaluation of proposed rate laws for mechanistic hypotheses testing.[224,225] The activation enthalpy and entropy of the rate-determining step of a catalytic reaction can be predicted by performing an Eyring analysis of computed rate constants, for direct comparison with experimental activation parameters.[225−227] Although using energies obtained by DFT is insufficient to predict absolute rates with high accuracy, smaller discrepancies compared with experiment should be obtained when estimating selectivities and relative abundances due to error cancellation (because they involve ratios of rates).[92]

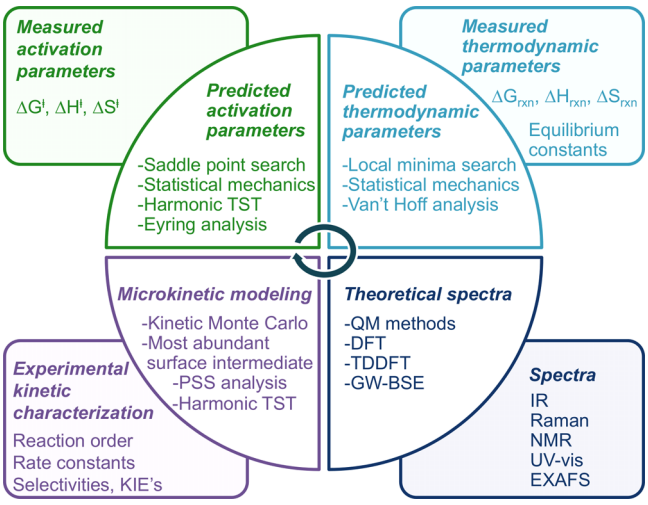

Figure 11. *Ab initio* computations for catalytic mechanisms (circle) should be vetted against measured thermodynamic, kinetic, and spectroscopic data (shaded squares). *Abbreviations:* KIE, kinetic isotope effect; PSS, pseudosteady state; QM, quantum mechanical; TDDFT, time-dependent DFT; GW-BSE, Green's function Bethe-Salpeter equation; TST, transition-state theory; Rxn, reaction.

DOI: 10.1021/acscatal.7b01767
ACS Catal. 2017, 7, 7543−7557

When computed quantities such as thermodynamic parameters, activation parameters, relative abundances, and kinetic isotope effects disagree with experimental observations and trends, then mechanistic hypotheses may require further scrutiny. In some cases, the computational model may be incorrect or insufficient. An unacceptable level of discrepancy can be estimated from typical errors generated by modern DFT hybrid exchange-correlation functionals of 10−30 kJ/mol for reaction free energies and activation free energies in non-charged systems at gas, liquid, and gas−solid interfaces.[228,229] Larger errors are expected for systems involving solid−liquid or charged interfaces, due to difficulty in modeling the solvent environment, describing the electronic-structure of charged species (due to delocalization error), and estimating partition functions. DFT computations should be benchmarked against more accurate electronic-structure methods whenever possible to give a better understanding of the magnitude and sources of errors for different classes of systems. Some DFT exchange-correlation functionals even provide computational error estimates using Bayesian statistics.[230,231]

4.2. Atomic-Level Characterization of Individual Sites.

Under operating conditions, catalysts undergo dynamic structural transformations to form active sites, underscoring the need to examine catalysts in real time.[27,232−234] *Operando* methods refer to characterizing a catalytic material during its exposure to realistic reaction conditions, and while its catalytic activity and selectivity are simultaneously measured.[235,236] When this powerful approach generates spectra with spatial and time resolution, it can elucidate the evolution of both active sites and reaction intermediates. For example, an electron paramagnetic resonance and DRUV−vis study by one of the authors showed that the $Cr(II)/SiO_2$ precursor state of the Phillips catalyst is immediately oxidized to $Cr(III)/SiO_2$ upon exposure to ethene.[237] As another example, a recent *operando* Raman, XANES, and EXAFS analysis of an amorphous cobalt sulfide electrocatalyst for H_2 evolution indicated that it transforms into highly active CoS_2-like molecular clusters in which cobalt is octahedrally coordinated by sulfur under cathodic polarization.[238]

Recent advances in characterization methods are giving researchers insight into the dynamic roles of the support under reaction conditions. For example, combined *in situ* transmission electron microscopy and DFT modeling enabled an atomically detailed description of oxide overlayer formation on Pd/TiO_2.[239] Amorphous TiO_x layers formed on Pd nanoparticles at low temperatures, followed by their crystallization into mono- or bilayer structures depending on the reaction conditions. Another study demonstrated that HCO_x adsorbates on Nb_2O_5- and TiO_2-supported Rh nanoparticle catalysts can drive oxygen vacancy formation in the support and induce the formation of a porous amorphous oxide overlayer on the Rh nanoparticle, which locally modifies the selectivity and activity of the underlying Rh surface.[124] Obtaining more detailed knowledge about these amorphous layers and other amorphous supports (e.g., the redox properties of amorphous Ce−Ti mixed oxides and amorphous CeO_2 for selective catalytic reduction of NO_x with NH_3)[240] will create opportunities to tune the properties of these important families of catalysts.

Comparison of results of *in situ*/*operando* experiments using supported molecular complexes as active site models with first-principles computational modeling can lead to mechanistic understanding about catalysis by amorphous solids.[241−243] The use of well-defined molecular complexes as catalyst components can aid in the development of structure−activity relationships. For example, two ^{13}C NMR signals were observed in the spectrum of CH_3ReO_3/silica−alumina.[103] A combination of mobility studies, selective grafting, and computational analysis was employed to assign the signals to the molecular complex associated with Brønsted and Lewis acid sites; the latter proved to be the sole source of the active sites in olefin metathesis. Isolated Co(II) species on silica were synthesized by grafting a cobalt silanolate precursor, followed by thermal treatment. Their reactivities were investigated using kinetic and *in situ* spectroscopic studies to probe the mechanisms of propane dehydrogenation, hydrogenation of propene, and the trimerization of terminal alkynes.[244] The reactions were suggested to occur via a common mechanism involving heterolytic C−H or H−H activation on a Co(II)−O bond, consistent with DFT calculations by Hu and co-workers.[245] In another example, a series of molecular Ga model complexes and silica-grafted surface organometallic Ga species were characterized using K-edge XANES.[246] It was suggested that during alkane dehydrogenation C−H bond activation occurs on Ga^{3+} active sites by a nonredox mechanism, involving gallium alkyl and hydride intermediates.

5. PROSPECTS

Although amorphous catalysts are well-established in chemical technology, they represent an emerging area for fundamental research in catalysis. In addition to well-known intrinsically amorphous materials, amorphous phases can also form from crystalline phases under reaction conditions. Advances in characterizing the dynamic behavior of both types of catalysts *in situ* and *operando* will likely lead to more examples and a better understanding of their consequences for reactivity. One such effect is subtle structural variability in dispersed metal ion sites which can lead to substantial changes in the rates of key elementary reaction steps, resulting in temperature-dependent changes in contributions to reactivity and stability. New approaches to describe this behavior accurately will require more than "single-site" models based on inflexible crystalline frameworks or rigid clusters, however "advanced". Until recently considered intractable, the problems of characterizing amorphous catalytic materials and understanding their heterogeneity are becoming solvable with powerful new methods that combine sophisticated and predictive models with dynamic experimental measurements.

AUTHOR INFORMATION

Corresponding Authors

*B.R.G.: tel, +1 734 764-3627; e-mail, bgoldsm@umich.edu.
*S.L.S.: tel, +1 805 893-5606; e-mail, sscott@engineering.ucsb.edu.

ORCID

Bryan R. Goldsmith: 0000-0003-1264-8018
J. Karl Johnson: 0000-0002-3608-8003
Bruce C. Gates: 0000-0003-0274-4882
Susannah L. Scott: 0000-0003-1161-0499

Notes

The authors declare no competing financial interest.

ACKNOWLEDGMENTS

S.L.S. and B.P. acknowledge support from the Catalysis Science Initiative of the U.S. Department of Energy (DOE), Basic Energy Sciences (BES) via grant DE-FG02-03ER15467. B.C.G.

DOI: 10.1021/acscatal.7b01767
ACS Catal. 2017, 7, 7543−7557

acknowledges support from DOE BES via grant DE-FG02-04ER15513. J.K.J. acknowledges support from DOE BES via grant DE-FG02-10ER16165. B.R.G. acknowledges support from the Alexander von Humboldt-Foundation via a Postdoctoral Fellowship. B.R.G. also thanks Markus Heyde at the Fritz Haber Institute of the Max Planck Society for fruitful discussions. B.P. thanks Richard Sear for stimulating discussions.

REFERENCES

(1) Taylor, H. S. *Proc. R. Soc. London, Ser. A* **1925**, *108*, 105−111.
(2) Ertl, G. *Angew. Chem., Int. Ed.* **2008**, *47*, 3524−3535.
(3) Zallen, R. *The Physics of Amorphous Solids*; Wiley: Mörlenbach, 2008; p 304.
(4) Yoon, C.; Cocke, D. L. *J. Non-Cryst. Solids* **1986**, *79*, 217−245.
(5) Cocke, D. L. *JOM* **1986**, *38*, 70−75.
(6) McDaniel, M. P. In *Advances in Catalysis*; Gates, B. C., Knözinger, H., Eds.; Elsiever: San Diego, 2010; Vol. *53*, pp 123−606.
(7) Morales-Guio, C. G.; Hu, X. *Acc. Chem. Res.* **2014**, *47*, 2671−2681.
(8) Peters, B.; Scott, S. L. *J. Chem. Phys.* **2015**, *142*, 104708.
(9) Howell, J. G.; Li, Y.-P.; Bell, A. T. *ACS Catal.* **2016**, *6*, 7728−7738.
(10) Brückner, R. *J. Non-Cryst. Solids* **1970**, *5*, 123−175.
(11) Brückner, R. *J. Non-Cryst. Solids* **1971**, *5*, 177−216.
(12) Sanz, J.; Fornés, V.; Corma, A. *J. Chem. Soc., Faraday Trans. 1* **1988**, *84*, 3113−3119.
(13) Menezes, S. M. C.; Camorim, V. L.; Lam, Y. L.; San Gil, R. A. S.; Bailly, A.; Amoureux, J. P. *Appl. Catal., A* **2001**, *207*, 367−377.
(14) Hoang-Van, C.; Teichner, S. J. *J. Catal.* **1970**, *16*, 69−74.
(15) Tavakoli, A. H.; Maram, P. S.; Widgeon, S. J.; Rufner, J.; van Benthem, K.; Ushakov, S.; Sen, S.; Navrotsky, A. *J. Phys. Chem. C* **2013**, *117*, 17123−17130.
(16) Ghorbel, A.; Hoang-Van, C.; Teichner, S. J. *J. Catal.* **1974**, *33*, 123−132.
(17) Ghorbel, A.; Hoang-Van, C.; Teichner, S. J. *J. Catal.* **1973**, *30*, 298−308.
(18) Busca, G. In *Advances in Catalysis*; Jentoft, F. C., Ed.; Academic Press: San Diego, 2014; Vol. *57*, pp 319−404.
(19) Digne, M.; Sautet, P.; Raybaud, P.; Euzen, P.; Toulhoat, H. *J. Catal.* **2004**, *226*, 54−68.
(20) Digne, M.; Sautet, P.; Raybaud, P.; Euzen, P.; Toulhoat, H. *J. Catal.* **2002**, *211*, 1−5.
(21) Xia, G. G.; Yin, Y. G.; Willis, W. S.; Wang, J. Y.; Suib, S. L. *J. Catal.* **1999**, *185*, 91−105.
(22) Musick, J. K.; Williams, F. W. *Ind. Eng. Chem., Prod. Res. Dev.* **1975**, *14*, 284−286.
(23) Jingfa, D.; Xiping, Z.; Enze, M. *Appl. Catal.* **1988**, *37*, 339−343.
(24) Li, H.; Li, H.; Dai, W.-L.; Wang, W.; Fang, Z.; Deng, J.-F. *Appl. Surf. Sci.* **1999**, *152*, 25−34.
(25) Konwar, L. J.; Boro, J.; Deka, D. *Renewable Sustainable Energy Rev.* **2014**, *29*, 546−564.
(26) Masa, J.; Weide, P.; Peeters, D.; Sinev, I.; Xia, W.; Sun, Z.; Somsen, C.; Muhler, M.; Schuhmann, W. *Adv. Energy Mater.* **2016**, *6*, 1502313.
(27) Hutchings, G. J.; Desmartin-Chomel, A.; Olier, R.; Volta, J.-C. *Nature* **1994**, *368*, 41−45.
(28) Goddard, W. A.; Liu, L.; Mueller, J. E.; Pudar, S.; Nielsen, R. J. *Top. Catal.* **2011**, *54*, 659−668.
(29) Grasselli, R. K.; Burrington, J. D.; Brazdil, J. F. *Faraday Discuss. Chem. Soc.* **1981**, *72*, 203−223.
(30) Bergmann, A.; Martinez-Moreno, E.; Teschner, D.; Chernev, P.; Gliech, M.; de Araujo, J. F.; Reier, T.; Dau, H.; Strasser, P. *Nat. Commun.* **2015**, *6*, 8625.
(31) Sholl, D. S.; Lively, R. P. *J. Phys. Chem. Lett.* **2015**, *6*, 3437−3444.
(32) Zachariasen, W. H. *J. Am. Chem. Soc.* **1932**, *54*, 3841−3851.
(33) Chuang, I. S.; Maciel, G. E. *J. Phys. Chem. B* **1997**, *101*, 3052−3064.
(34) Rozanska, X.; Delbecq, F.; Sautet, P. *Phys. Chem. Chem. Phys.* **2010**, *12*, 14930−14940.
(35) Quadrelli, E. A.; Basset, J.-M. *Coord. Chem. Rev.* **2010**, *254*, 707−728.
(36) Feher, F. J.; Newman, D. A.; Walzer, J. F. *J. Am. Chem. Soc.* **1989**, *111*, 1741−1748.
(37) Fraile, J. M.; García, J. I.; Mayoral, J. A.; Vispe, E. *J. Catal.* **2005**, *233*, 90−99.
(38) Guillo, P.; Lipschutz, M. I.; Fasulo, M. E.; Tilley, T. D. *ACS Catal.* **2017**, *7*, 2303−2312.
(39) Josephson, T. R.; Brand, S. K.; Caratzoulas, S.; Vlachos, D. G. *ACS Catal.* **2017**, *7*, 25−33.
(40) Cordes, D. B.; Lickiss, P. D.; Rataboul, F. *Chem. Rev.* **2010**, *110*, 2081−2173.
(41) *Challenges at the Frontiers of Matter and Energy: Transformative Opportunities for Discovery Science*; USDOE Office of Science (United States): Washington, DC, 2015; p 78.
(42) Kanan, M. W.; Surendranath, Y.; Nocera, D. G. *Chem. Soc. Rev.* **2009**, *38*, 109−114.
(43) Leydier, F.; Chizallet, C.; Costa, D.; Raybaud, P. *Chem. Commun.* **2012**, *48*, 4076−4078.
(44) Ewing, C. S.; Hartmann, M. J.; Martin, K. R.; Musto, A. M.; Padinjarekutt, S. J.; Weiss, E. M.; Veser, G.; McCarthy, J. J.; Johnson, J. K.; Lambrecht, D. S. *J. Phys. Chem. C* **2015**, *119*, 2503−2512.
(45) Gates, B. *Chem. Rev.* **1995**, *95*, 511−522.
(46) Rascón, F.; Wischert, R.; Copéret, C. *Chem. Sci.* **2011**, *2*, 1449−1456.
(47) Mol, J. C. *J. Mol. Catal. A: Chem.* **2004**, *213*, 39−45.
(48) Sushko, P. V.; Mukhopadhyay, S.; Mysovsky, A. S.; Sulimov, V. B.; Taga, A.; Shluger, A. L. *J. Phys.: Condens. Matter* **2005**, *17*, S2115.
(49) Bergna, H. E. *The Colloid Chemistry of Silica*; American Chemical Society: Washington, DC, 1994.
(50) Iler, R. K. *The Chemistry of Silica: Solubility, Polymerization, Colloid and Surface Properties, and Biochemistry*; Wiley: New York, 1979.
(51) Papirer, E. *Adsorption on Silica Surfaces*; CRC Press: Boca Raton, FL, 2000; Vol. *90*.
(52) Lichtenstein, L.; Büchner, C.; Yang, B.; Shaikhutdinov, S.; Heyde, M.; Sierka, M.; Włodarczyk, R.; Sauer, J.; Freund, H.-J. *Angew. Chem., Int. Ed.* **2012**, *51*, 404−407.
(53) Büchner, C.; Lichtenstein, L.; Heyde, M.; Freund, H.-J. In *Noncontact Atomic Force Microscopy*; Springer: Berlin, 2015; pp 327−353.
(54) Büchner, C.; Liu, L.; Stuckenholz, S.; Burson, K. M.; Lichtenstein, L.; Heyde, M.; Gao, H.-J.; Freund, H.-J. *J. Non-Cryst. Solids* **2016**, *435*, 40−47.
(55) Bell, R. J.; Dean, P. *Philos. Mag.* **1972**, *25*, 1381−1398.
(56) Shackelford, J. F.; Brown, B. D. *J. Non-Cryst. Solids* **1981**, *44*, 379−382.
(57) Demmelmaier, C. A.; White, R. E.; van Bokhoven, J. A.; Scott, S. L. *J. Catal.* **2009**, *262*, 44−56.
(58) Das, U.; Zhang, G.; Hu, B.; Hock, A. S.; Redfern, P. C.; Miller, J. T.; Curtiss, L. A. *ACS Catal.* **2015**, *5*, 7177−7185.
(59) Goldsmith, B. R.; Sanderson, E. D.; Bean, D.; Peters, B. *J. Chem. Phys.* **2013**, *138*, 204105.
(60) Yu, X.; Emmez, E.; Pan, Q.; Yang, B.; Pomp, S.; Kaden, W. E.; Sterrer, M.; Shaikhutdinov, S.; Freund, H.-J.; Goikoetxea, I.; Wlodarczyk, R.; Sauer, J. *Phys. Chem. Chem. Phys.* **2016**, *18*, 3755−3764.
(61) Scherzer, J.; Gruia, A. J. *Hydrocracking science and technology*; CRC Press: Boca Raton, FL, 1996.
(62) Carberry, J. J. *Chemical and Catalytic Reaction Engineering*; Dover: Minneola, NY, 2001.
(63) Abbattista, F.; Delmastro, S.; Gozzelino, G.; Mazza, D.; Vallino, M.; Busca, G.; Lorenzelli, V.; Ramis, G. *J. Catal.* **1989**, *117*, 42−51.

DOI: 10.1021/acscatal.7b01767
ACS Catal. 2017, 7, 7543−7557

(64) Abbattista, F.; Delmastro, A.; Gozzelino, G.; Mazza, D.; Vallino, M.; Busca, G.; Lorenzelli, V. *J. Chem. Soc., Faraday Trans.* **1990**, *86*, 3653−3658.
(65) Delmastro, A.; Gozzelino, G.; Mazza, D.; Vallino, M.; Busca, G.; Lorenzelli, V. *J. Chem. Soc., Faraday Trans.* **1992**, *88*, 2065−2070.
(66) Chen, F.; Davis, J.; Fripiat, J. *J. Catal.* **1992**, *133*, 263−278.
(67) Adiga, S. P.; Zapol, P.; Curtiss, L. A. *J. Phys. Chem. C* **2007**, *111*, 7422−7429.
(68) Krokidis, X.; Raybaud, P.; Gobichon, A.-E.; Rebours, B.; Euzen, P.; Toulhoat, H. *J. Phys. Chem. B* **2001**, *105*, 5121−5130.
(69) Adiga, S. P.; Zapol, P.; Curtiss, L. A. *Phys. Rev. B: Condens. Matter Mater. Phys.* **2006**, *74*, 064204.
(70) Wischert, R.; Florian, P.; Copéret, C.; Massiot, D.; Sautet, P. *J. Phys. Chem. C* **2014**, *118*, 15292−15299.
(71) Sohlberg, K.; Pennycook, S. J.; Pantelides, S. T. *Chem. Eng. Commun.* **2000**, *181*, 107−135.
(72) Hahn, M. W.; Copeland, J. R.; van Pelt, A. H.; Sievers, C. *ChemSusChem* **2013**, *6*, 2304−2315.
(73) Corma, A.; Grande, M. S.; Gonzalez-Alfaro, V.; Orchilles, A. V. *J. Catal.* **1996**, *159*, 375−382.
(74) Crépeau, G.; Montouillout, V.; Vimont, A.; Mariey, L.; Cseri, T.; Maugé, F. *J. Phys. Chem. B* **2006**, *110*, 15172−15185.
(75) Chizallet, C.; Raybaud, P. *Angew. Chem., Int. Ed.* **2009**, *48*, 2891−2893.
(76) Chizallet, C.; Raybaud, P. *ChemPhysChem* **2010**, *11*, 105−108.
(77) Leydier, F.; Chizallet, C.; Costa, D.; Raybaud, P. *J. Catal.* **2015**, *325*, 35−47.
(78) Trombetta, M.; Busca, G.; Rossini, S.; Piccoli, V.; Cornaro, U.; Guercio, A.; Catani, R.; Willey, R. J. *J. Catal.* **1998**, *179*, 581−596.
(79) Daniell, W.; Schubert, U.; Glöckler, R.; Meyer, A.; Noweck, K.; Knözinger, H. *Appl. Catal., A* **2000**, *196*, 247−260.
(80) Góra-Marek, K.; Datka, J. *Appl. Catal., A* **2006**, *302*, 104−109.
(81) Xu, B.; Sievers, C.; Lercher, J. A.; van Veen, J. A. R.; Giltay, P.; Prins, R.; van Bokhoven, J. A. *J. Phys. Chem. C* **2007**, *111*, 12075−12079.
(82) Hensen, E. J. M.; Poduval, D. G.; Degirmenci, V.; Ligthart, D. A. J. M.; Chen, W.; Maugé, F.; Rigutto, M. S.; van Veen, J. A. R. *J. Phys. Chem. C* **2012**, *116*, 21416−21429.
(83) Begley, J.; Wilson, R. *J. Catal.* **1967**, *9*, 375−395.
(84) Lwin, S.; Wachs, I. E. *ACS Catal.* **2014**, *4*, 2505−2520.
(85) Lwin, S.; Li, Y.; Frenkel, A. I.; Wachs, I. E. *ACS Catal.* **2015**, *5*, 6807−6814.
(86) Regalbuto, J. *Catalyst Preparation: Science and Engineering*; CRC Press: Boca Raton, FL, 2016; p 488.
(87) Pelletier, J. D. A.; Basset, J.-M. *Acc. Chem. Res.* **2016**, *49*, 664−677.
(88) Tranca, D. C.; Wojtaszek-Gurdak, A.; Ziolek, M.; Tielens, F. *Phys. Chem. Chem. Phys.* **2015**, *17*, 22402−22411.
(89) Fong, A.; Yuan, Y.; Ivry, S. L.; Scott, S. L.; Peters, B. *ACS Catal.* **2015**, *5*, 3360−3374.
(90) Gierada, M.; Michorczyk, P.; Tielens, F.; Handzlik, J. *J. Catal.* **2016**, *340*, 122−135.
(91) Floryan, L.; Borosy, A. P.; Núñez-Zarur, F.; Comas-Vives, A.; Copéret, C. *J. Catal.* **2017**, *346*, 50−56.
(92) Peters, B.; Scott, S. L.; Fong, A.; Wang, Y.; Stiegman, A. E. *Proc. Natl. Acad. Sci. U. S. A.* **2015**, *112*, E4160−E4161.
(93) Delley, M. F.; Núñez-Zarur, F.; Conley, M. P.; Comas-Vives, A.; Siddiqi, G.; Norsic, S.; Monteil, V.; Safonova, O. V.; Copéret, C. *Proc. Natl. Acad. Sci. U. S. A.* **2014**, *111*, 11624−11629.
(94) Yao, N.; Xiong, G.; He, M.; Sheng, S.; Yang, W.; Bao, X. *Chem. Mater.* **2002**, *14*, 122−129.
(95) Conley, M. P.; Delley, M. F.; Núñez-Zarur, F.; Comas-Vives, A.; Copéret, C. *Inorg. Chem.* **2015**, *54*, 5065−5078.
(96) Fong, A.; Peters, B.; Scott, S. L. *ACS Catal.* **2016**, *6*, 6073−6085.
(97) Brown, C. E.; Stiegman, A. E.; Callahan, S.; Achey, R. M.; Fu, R. Q. *Abstr. Pap. Am. Chem. Soc.* 2006, *231*, Abstract No. INOR-435
(98) Brown, C.; Krzystek, J.; Fu, R.; Meulenberg, R. W.; Scott, S. L.; Stiegman, A. E. *The Mechanism of the Phillips Ethylene Polymerization Catalyst*; 24th North American Meeting of the Catalysis Society, Pittsburgh, PA, June 14−19, 2015.
(99) Brown, C.; Lita, A.; Tao, Y.; Peek, N.; Crosswhite, M.; Mileham, M.; Krzystek, J.; Achey, R.; Fu, R.; Kaur, J.; Polinski, M.; Wang, Y.; J. van de Burgt, L.; Jeffcoat, D.; Profeta, S., Jr.; Stiegman, A. E.; Scott, S. L. *ACS Catal.*, 2017.
(100) Conley, M. P.; Delley, M. F.; Núñez-Zarur, F.; Comas-Vives, A.; Copéret, C. *Inorg. Chem.* **2015**, *54*, 5065−5078.
(101) Herrmann, W. A.; Wagner, W.; Flessner, U. N.; Volkhardt, U.; Komber, H. *Angew. Chem., Int. Ed. Engl.* **1991**, *30*, 1636−1638.
(102) Morris, L. J.; Downs, A. J.; Greene, T. M.; McGrady, G. S.; Herrmann, W. A.; Sirsch, P.; Scherer, W.; Gropen, O. *Organometallics* **2001**, *20*, 2344−2352.
(103) Moses, A. W.; Raab, C.; Nelson, R. C.; Leifeste, H. D.; Ramsahye, N. A.; Chattopadhyay, S.; Eckert, J.; Chmelka, B. F.; Scott, S. L. *J. Am. Chem. Soc.* **2007**, *129*, 8912−8920.
(104) Mathew, T. M.; du Plessis, J. A. K.; Prinsloo, J. J. *J. Mol. Catal. A: Chem.* **1999**, *148*, 157−164.
(105) Moses, A. W.; Ramsahye, N. A.; Raab, C.; Leifeste, H. D.; Chattopadhyay, S.; Chmelka, B. F.; Eckert, J.; Scott, S. L. *Organometallics* **2006**, *25*, 2157−2165.
(106) Wischert, R.; Copéret, C.; Delbecq, F.; Sautet, P. *ChemCatChem* **2010**, *2*, 812−815.
(107) Gallo, A.; Fong, A.; Szeto, K. C.; Rieb, J.; Delevoye, L.; Gauvin, R. M.; Taoufik, M.; Peters, B.; Scott, S. L. *J. Am. Chem. Soc.* **2016**, *138*, 12935−12947.
(108) Valla, M.; Wischert, R.; Comas-Vives, A.; Conley, M. P.; Verel, R.; Copéret, C.; Sautet, P. *J. Am. Chem. Soc.* **2016**, *138*, 6774.
(109) Bein, T.; Huber, C.; Moller, K.; Wu, C.-G.; Xu, L. *Chem. Mater.* **1997**, *9*, 2252−2254.
(110) Rost, A. M. J.; Schneider, H.; Zoller, J. P.; Herrmann, W. A.; Kühn, F. E. *J. Organomet. Chem.* **2005**, *690*, 4712−4718.
(111) Salameh, A.; Baudouin, A.; Soulivong, D.; Boehm, V.; Roeper, M.; Basset, J.-M.; Copéret, C. *J. Catal.* **2008**, *253*, 180−190.
(112) Salameh, A.; Joubert, J.; Baudouin, A.; Lukens, W.; Delbecq, F.; Sautet, P.; Basset, J. M.; Coperet, C. *Angew. Chem., Int. Ed.* **2007**, *46*, 3870−3873.
(113) Kulkarni, A.; Lobo-Lapidus, R. J.; Gates, B. C. *Chem. Commun.* **2010**, *46*, 5997−6015.
(114) Vajda, S.; White, M. G. *ACS Catal.* **2015**, *5*, 7152−7176.
(115) Meyer, R.; Lei, Y.; Lee, S.; Vajda, S. In *Model Systems in Catalysis: Single Crystals to Supported Enzyme Mimics*; Rioux, R., Ed.; Springer: New York, 2010; pp 345−365.
(116) Xu, Z.; Xiao, F. S.; Purnell, S. K.; Alexeev, O.; Kawi, S.; Deutsch, S. E.; Gates, B. C. *Nature* **1994**, *372*, 346−348.
(117) Taketoshi, A.; Haruta, M. *Chem. Lett.* **2014**, *43*, 380−387.
(118) Schauermann, S.; Nilius, N.; Shaikhutdinov, S.; Freund, H.-J. *Acc. Chem. Res.* **2013**, *46*, 1673−1681.
(119) Ertl, G.; Knözinger, H.; Schüth, F.; Weitkamp, J., Eds. *Handbook of Heterogeneous Catalysis*, 2nd ed., Vol. *8*; Wiley: Weinheim, 2008.
(120) Bell, A. T. *Science* **2003**, *299*, 1688−1691.
(121) Wynblatt, P.; Gjostein, N. *Acta Metall.* **1976**, *24*, 1165−1174.
(122) Parker, S. C.; Campbell, C. T. *Phys. Rev. B: Condens. Matter Mater. Phys.* **2007**, *75*, 035430.
(123) Goldsmith, B. R.; Sanderson, E. D.; Ouyang, R.; Li, W.-X. *J. Phys. Chem. C* **2014**, *118*, 9588−9597.
(124) Matsubu, J. C.; Zhang, S.; DeRita, L.; Marinkovic, N. S.; Chen, J. G.; Graham, G. W.; Pan, X.; Christopher, P. *Nat. Chem.* **2017**, *9*, 120−127.
(125) Ouyang, R.; Liu, J.-X.; Li, W.-X. *J. Am. Chem. Soc.* **2013**, *135*, 1760−1771.
(126) Hansen, T. W.; DeLaRiva, A. T.; Challa, S. R.; Datye, A. K. *Acc. Chem. Res.* **2013**, *46*, 1720−1730.
(127) Matsubu, J. C.; Yang, V. N.; Christopher, P. *J. Am. Chem. Soc.* **2015**, *137*, 3076−3084.
(128) Parkinson, G. S.; Novotny, Z.; Argentero, G.; Schmid, M.; Pavelec, J.; Kosak, R.; Blaha, P.; Diebold, U. *Nat. Mater.* **2013**, *12*, 724−728.

DOI: 10.1021/acscatal.7b01767
ACS Catal. 2017, 7, 7543−7557

(129) Peterson, E. J.; DeLaRiva, A. T.; Lin, S.; Johnson, R. S.; Guo, H.; Miller, J. T.; Hun Kwak, J.; Peden, C. H. F.; Kiefer, B.; Allard, L. F.; Ribeiro, F. H.; Datye, A. K. *Nat. Commun.* **2014**, *5*, 4885.
(130) Jones, J.; Xiong, H.; DeLaRiva, A. T.; Peterson, E. J.; Pham, H.; Challa, S. R.; Qi, G.; Oh, S.; Wiebenga, M. H.; Hernández, X. I. P.; et al. *Science* **2016**, *353*, 150−154.
(131) Freund, H.-J.; Meijer, G.; Scheffler, M.; Schlögl, R.; Wolf, M. *Angew. Chem., Int. Ed.* **2011**, *50*, 10064−10094.
(132) Zwanzig, R. *Acc. Chem. Res.* **1990**, *23*, 148−152.
(133) Häkkinen, H.; Abbet, S.; Sanchez, A.; Heiz, U.; Landman, U. *Angew. Chem., Int. Ed.* **2003**, *42*, 1297−1300.
(134) Mingos, D. M. P., Ed. *Gold Clusters, Colloids and Nanoparticles I*; Springer: Berlin, 2014; Vol. *161*, p 282.
(135) Palacios, F. J.; Iñiguez, M. P.; López, M. J.; Alonso, J. A. *Phys. Rev. B: Condens. Matter Mater. Phys.* **1999**, *60*, 2908−2915.
(136) Lobo-Lapidus, R. J.; Gates, B. C. *J. Catal.* **2009**, *268*, 89−99.
(137) Alexeev, O. S.; Panjabi, G.; Phillips, B. L.; Gates, B. C. *Langmuir* **2003**, *19*, 9494−9503.
(138) Argo, A. M.; Odzak, J. F.; Gates, B. C. *J. Am. Chem. Soc.* **2003**, *125*, 7107−7115.
(139) Fung, A. S.; Tooley, P. A.; Kelley, M. J.; Koningsberger, D. C.; Gates, B. C. *J. Phys. Chem.* **1991**, *95*, 225−234.
(140) Koningsberger, D. C.; Gates, B. C. *Catal. Lett.* **1992**, *14*, 271−277.
(141) Vayssilov, G. N.; Gates, B. C.; Rösch, N. *Angew. Chem., Int. Ed.* **2003**, *42*, 1391−1394.
(142) Binns, C. *Surf. Sci. Rep.* **2001**, *44*, 1−49.
(143) Molina, L. M.; Lee, S.; Sell, K.; Barcaro, G.; Fortunelli, A.; Lee, B.; Seifert, S.; Winans, R. E.; Elam, J. W.; Pellin, M. J.; Barke, I.; von Oeynhausen, V.; Lei, Y.; Meyer, R. J.; Alonso, J. A.; Fraile Rodríguez, A.; Kleibert, A.; Giorgio, S.; Henry, C. R.; Meiwes-Broer, K.-H.; Vajda, S. *Catal. Today* **2011**, *160*, 116−130.
(144) Handzlik, J.; Grybos, R.; Tielens, F. *J. Phys. Chem. C* **2013**, *117*, 8138−8149.
(145) Comas-Vives, A.; Larmier, K.; Copéret, C. *Chem. Commun.* **2017**, *53*, 4296−4303.
(146) Gierada, M.; Handzlik, J. *J. Catal.* **2017**, *352*, 314−328.
(147) Handzlik, J.; Ogonowski, J. *J. Phys. Chem. C* **2012**, *116*, 5571−5584.
(148) Guesmi, H.; Gryboś, R.; Handzlik, J.; Tielens, F. *Phys. Chem. Chem. Phys.* **2014**, *16*, 18253−18260.
(149) Guesmi, H.; Gryboś, R.; Handzlik, J.; Tielens, F. *RSC Adv.* **2016**, *6*, 39424−39432.
(150) Curtiss, L. A.; Gordon, M. S. *Computational Materials Chemistry: Methods and Applications*. Springer: Berlin, 2004.
(151) van Santen, R. A. *J. Mol. Catal. A: Chem.* **1997**, *115*, 405−419.
(152) Nascimento, M. *Theoretical Aspects of Heterogeneous Catalysis*; Springer: Berlin, 2006; Vol. *8*.
(153) Møller, C.; Plesset, M. S. *Phys. Rev.* **1934**, *46*, 618−622.
(154) Jensen, F. *Introduction to Computational Chemistry*, 2nd ed.; Wiley: 2013.
(155) Ren, X.; Rinke, P.; Joas, C.; Scheffler, M. *J. Mater. Sci.* **2012**, *47*, 7447−7471.
(156) Cohen, A. J.; Mori-Sánchez, P.; Yang, W. *Chem. Rev.* **2012**, *112*, 289−320.
(157) Koch, W.; Holthausen, M. C. *A Chemist's Guide to Density Functional Theory*; John Wiley & Sons: Hoboken, NJ, 2015.
(158) Ewing, C. S.; Bagusetty, A.; Patriarca, E. G.; Lambrecht, D. S.; Veser, G.; Johnson, J. K. *Ind. Eng. Chem. Res.* **2016**, *55*, 12350−12357.
(159) Vollmer, J. M.; Stefanovich, E. V.; Truong, T. N. *J. Phys. Chem. B* **1999**, *103*, 9415−9422.
(160) Espelid, Ø.; Børve, K. J. *Catal. Lett.* **2002**, *75*, 49−54.
(161) Magg, N.; Immaraporn, B.; Giorgi, J. B.; Schroeder, T.; Bäumer, M.; Döbler, J.; Wu, Z.; Kondratenko, E.; Cherian, M.; Baerns, M.; Stair, P. C.; Sauer, J.; Freund, H.-J. *J. Catal.* **2004**, *226*, 88−100.
(162) Bell, A. T.; Head-Gordon, M. *Annu. Rev. Chem. Biomol. Eng.* **2011**, *2*, 453−477.
(163) Duchateau, R. *Chem. Rev.* **2002**, *102*, 3525−3542.
(164) Michalske, T. A.; Bunker, B. *J. Appl. Phys.* **1984**, *56*, 2686−2693.
(165) Goldsmith, B. R.; Fong, A.; Peters, B. In *Reaction Rate Constant Computations: Theories and Applications*; Royal Society of Chemistry: London, 2013; Vol. *6*, pp 213−232.
(166) Van Ginhoven, R. M.; Jónsson, H.; Corrales, L. R. *Phys. Rev. B: Condens. Matter Mater. Phys.* **2005**, *71*, 024208.
(167) Dharma-wardana, M. W. C.; Zgierski, M. Z.; Ritchie, D.; Ping, J. G.; Ruda, H. *Phys. Rev. B: Condens. Matter Mater. Phys.* **1999**, *59*, 15766−15771.
(168) Teunissen, E. H.; Roetti, C.; Pisani, C.; Man, A. J. M. d.; Jansen, A. P. J.; Orlando, R.; Santen, R. A. v.; Dovesi, R. *Modell. Simul. Mater. Sci. Eng.* **1994**, *2*, 921.
(169) Steckel, J.; Phung, T.; Jordan, K. D.; Nachtigall, P. *J. Phys. Chem. B* **2001**, *105*, 4031−4038.
(170) Handzlik, J. *J. Phys. Chem. C* **2007**, *111*, 9337−9348.
(171) Ugliengo, P.; Sodupe, M.; Musso, F.; Bush, I. J.; Orlando, R.; Dovesi, R. *Adv. Mater.* **2008**, *20*, 4579−4583.
(172) Adiga, S.; Zapol, P.; Curtiss, L. *Phys. Rev. B: Condens. Matter Mater. Phys.* **2006**, *74*, 064204.
(173) Adiga, S.; Zapol, P.; Curtiss, L. *J. Phys. Chem. C* **2007**, *111*, 7422−7429.
(174) Ewing, C. S.; Bhavsar, S.; Veser, G.; McCarthy, J. J.; Johnson, J. K. *Langmuir* **2014**, *30*, 5133−5141.
(175) Berger, D.; Logsdail, A. J.; Oberhofer, H.; Farrow, M. R.; Catlow, C. R. A.; Sherwood, P.; Sokol, A. A.; Blum, V.; Reuter, K. *J. Chem. Phys.* **2014**, *141*, 024105.
(176) Chung, L. W.; Sameera, W. M. C.; Ramozzi, R.; Page, A. J.; Hatanaka, M.; Petrova, G. P.; Harris, T. V.; Li, X.; Ke, Z.; Liu, F.; Li, H.-B.; Ding, L.; Morokuma, K. *Chem. Rev.* **2015**, *115*, 5678−5796.
(177) Lizárraga, R.; Holmström, E.; Parker, S. C.; Arrouvel, C. *Phys. Rev. B: Condens. Matter Mater. Phys.* **2011**, *83*, 094201.
(178) Schumacher, C.; Gonzalez, J.; Wright, P. A.; Seaton, N. A. *J. Phys. Chem. B* **2006**, *110*, 319−333.
(179) Feuston, B.; Higgins, J. *J. Phys. Chem.* **1994**, *98*, 4459−4462.
(180) Maddox, M.; Olivier, J.; Gubbins, K. *Langmuir* **1997**, *13*, 1737−1745.
(181) Gierada, M.; Petit, I.; Handzlik, J.; Tielens, F. *Phys. Chem. Chem. Phys.* **2016**, *18*, 32962−32972.
(182) Schacht, S.; Janicke, M.; Schüth, F. *Microporous Mesoporous Mater.* **1998**, *22*, 485−493.
(183) Joly, J.-F.; Béland, L. K.; Brommer, P.; Mousseau, N. *Phys. Rev. B: Condens. Matter Mater. Phys.* **2013**, *87*, 144204.
(184) Barkema, G.; Mousseau, N. *Phys. Rev. Lett.* **1996**, *77*, 4358.
(185) Keen, D. A.; McGreevy, R. L. *Nature* **1990**, *344*, 423−425.
(186) Keen, D. A.; Tucker, M. G.; Dove, M. T. *J. Phys.: Condens. Matter* **2005**, *17*, S15.
(187) Keen, D. A. *Phase Transitions* **1997**, *61*, 109−124.
(188) Chizallet, C.; Raybaud, P. *Catal. Sci. Technol.* **2014**, *4*, 2797−2813.
(189) Duchateau, R.; Harmsen, R. J.; Abbenhuis, H. C. L.; van Santen, R. A.; Meetsma, A.; Thiele, S. K. H.; Kranenburg, M. *Chem. - Eur. J.* **1999**, *5*, 3130−3135.
(190) Pfeiffer-Laplaud, M.; Costa, D.; Tielens, F.; Gaigeot, M.-P.; Sulpizi, M. *J. Phys. Chem. C* **2015**, *119*, 27354−27362.
(191) Tielens, F.; Gervais, C.; Lambert, J. F.; Mauri, F.; Costa, D. *Chem. Mater.* **2008**, *20*, 3336−3344.
(192) Vansant, E. F.; Van Der Voort, P.; Vrancken, K. C. *Characterization and Chemical Modification of the Silica Surface*. Elsevier: Amsterdam, 1995.
(193) Zhuravlev, L. T. *Colloids Surf., A* **2000**, *173*, 1−38.
(194) Comas-Vives, A. *Phys. Chem. Chem. Phys.* **2016**, *18*, 7475−7482.
(195) Fleischman, S. D.; Scott, S. L. *J. Am. Chem. Soc.* **2011**, *133*, 4847−4855.
(196) Scott, S. L.; Basset, J.-M. *J. Am. Chem. Soc.* **1994**, *116*, 12069−12070.
(197) Morrow, B. A.; McFarlan, A. J. *Langmuir* **1991**, *7*, 1695−1701.

DOI: 10.1021/acscatal.7b01767
ACS Catal. 2017, 7, 7543−7557

(198) Morrow, B. A.; McFarlan, A. J. *J. Phys. Chem.* **1992**, *96*, 1395−1400.
(199) Ewing, C. S.; Veser, G.; McCarthy, J. J.; Lambrecht, D. S.; Johnson, J. K. *Surf. Sci.* **2016**, *652*, 278−285.
(200) Constable, F. H. *Proc. R. Soc. London, Ser. A* **1925**, *108*, 355−378.
(201) Cohen, A. J.; Mori-Sánchez, P.; Yang, W. *Science* **2008**, *321*, 792−794.
(202) Senftle, T. P.; Hong, S.; Islam, M. M.; Kylasa, S. B.; Zheng, Y.; Shin, Y. K.; Junkermeier, C.; Engel-Herbert, R.; Janik, M. J.; Aktulga, H. M.; Verstraelen, T.; Grama, A.; van Duin, A. C. T. *npj Comput. Mater.* **2016**, *2*, 15011.
(203) Behler, J. *Phys. Chem. Chem. Phys.* **2011**, *13*, 17930−17955.
(204) Rupp, M. *Int. J. Quantum Chem.* **2015**, *115*, 1058−1073.
(205) Artrith, N.; Urban, A.; Ceder, G. 2017, *arXiv preprint arXiv:1706.06293*. arXiv e-Print archive. https://arxiv.org/abs/1706.06293.
(206) Ma, X.; Li, Z.; Achenie, L. E.; Xin, H. *J. Phys. Chem. Lett.* **2015**, *6*, 3528−3533.
(207) Isayev, O.; Oses, C.; Toher, C.; Gossett, E.; Curtarolo, S.; Tropsha, A. *Nat. Commun.* **2017**, *8*, 15679.
(208) Curtarolo, S.; Setyawan, W.; Hart, G. L.; Jahnatek, M.; Chepulskii, R. V.; Taylor, R. H.; Wang, S.; Xue, J.; Yang, K.; Levy, O.; et al. *Comput. Mater. Sci.* **2012**, *58*, 218−226.
(209) Ghiringhelli, L. M.; Vybiral, J.; Levchenko, S. V.; Draxl, C.; Scheffler, M. *Phys. Rev. Lett.* **2015**, *114*, 105503.
(210) Mueller, T.; Johlin, E.; Grossman, J. C. *Phys. Rev. B: Condens. Matter Mater. Phys.* **2014**, *89*, 115202.
(211) Goldsmith, B. R.; Boley, M.; Vreeken, J.; Scheffler, M.; Ghiringhelli, L. M. *New J. Phys.* **2017**, *19*, 013031.
(212) Boley, M.; Goldsmith, B. R.; Ghiringhelli, L. M.; Vreeken, J. *Data Min. Knowl. Disc.* **2017**, *31*, 1391−1418.
(213) Liu, F. T.; Ting, K. M.; Zhou, Z.-H. *Isolation forest*, Data Mining, 2008. ICDM '08. Eighth IEEE International Conference on Data Mining, Pisa, Italy, December 15−19, 2008; pp 413−422.
(214) Rousseeuw, P. J.; Driessen, K. V. *Technometrics* **1999**, *41*, 212−223.
(215) Ulissi, Z. W.; Medford, A. J.; Bligaard, T.; Nørskov, J. K. *Nat. Commun.* **2017**, *8*, 14621.
(216) Peterson, A. A. *J. Chem. Phys.* **2016**, *145*, 074106.
(217) Pozun, Z. D.; Hansen, K.; Sheppard, D.; Rupp, M.; Müller, K.-R.; Henkelman, G. *J. Chem. Phys.* **2012**, *136*, 174101.
(218) Ghiringhelli, L. M.; Carbogno, C.; Levchenko, S.; Mohamed, F.; Huhs, G.; Lüders, M.; Oliveira, M.; Scheffler, M. 2016, *arXiv preprint arXiv:1607.04738*. arXiv e-Print archive. https://arxiv.org/abs/1607.04738.
(219) Hummelshøj, J. S.; Abild-Pedersen, F.; Studt, F.; Bligaard, T.; Nørskov, J. K. *Angew. Chem.* **2012**, *124*, 278−280.
(220) Jain, A.; Ong, S. P.; Hautier, G.; Chen, W.; Richards, W. D.; Dacek, S.; Cholia, S.; Gunter, D.; Skinner, D.; Ceder, G.; Persson, K. A. *APL Mater.* **2013**, *1*, 011002.
(221) Curtarolo, S.; Setyawan, W.; Wang, S.; Xue, J.; Yang, K.; Taylor, R. H.; Nelson, L. J.; Hart, G. L. W.; Sanvito, S.; Buongiorno-Nardelli, M.; Mingo, N.; Levy, O. *Comput. Mater. Sci.* **2012**, *58*, 227−235.
(222) Bligaard, T.; Bullock, R. M.; Campbell, C. T.; Chen, J. G.; Gates, B. C.; Gorte, R. J.; Jones, C. W.; Jones, W. D.; Kitchin, J. R.; Scott, S. L. *ACS Catal.* **2016**, *6*, 2590−2602.
(223) Truhlar, D. G.; Garrett, B. C.; Klippenstein, S. J. *J. Phys. Chem.* **1996**, *100*, 12771−12800.
(224) Boudart, M.; Djéga-Mariadassou, G. *Kinetics of Heterogeneous Catalytic Reactions*. Princeton University Press: Princeton, 1984; p 242.
(225) Peters, B. *J. Phys. Chem. B* **2015**, *119*, 6349−6356.
(226) Goldsmith, B. R.; Hwang, T.; Seritan, S.; Peters, B.; Scott, S. L. *J. Am. Chem. Soc.* **2015**, *137*, 9604−9616.
(227) Hwang, T.; Goldsmith, B. R.; Peters, B.; Scott, S. L. *Inorg. Chem.* **2013**, *52*, 13904−13917.
(228) Zhao, Y.; Truhlar, D. G. *J. Chem. Theory Comput.* **2011**, *7*, 669−676.
(229) Hu, L.; Chen, H. *J. Chem. Theory Comput.* **2015**, *11*, 4601−4614.
(230) Wellendorff, J.; Lundgaard, K. T.; Møgelhøj, A.; Petzold, V.; Landis, D. D.; Nørskov, J. K.; Bligaard, T.; Jacobsen, K. W. *Phys. Rev. B: Condens. Matter Mater. Phys.* **2012**, *85*, 235149.
(231) Mortensen, J. J.; Kaasbjerg, K.; Frederiksen, S. L.; Nørskov, J. K.; Sethna, J. P.; Jacobsen, K. W. *Phys. Rev. Lett.* **2005**, *95*, 216401.
(232) Kale, M. J.; Christopher, P. *ACS Catal.* **2016**, *6*, 5599−5609.
(233) Casalongue, H. G. S.; Benck, J. D.; Tsai, C.; Karlsson, R. K.; Kaya, S.; Ng, M. L.; Pettersson, L. G.; Abild-Pedersen, F.; Nørskov, J.; Ogasawara, H.; et al. *J. Phys. Chem. C* **2014**, *118*, 29252−29259.
(234) Kondrat, S. A.; Smith, P. J.; Wells, P. P.; Chater, P. A.; Carter, J. H.; Morgan, D. J.; Fiordaliso, E. M.; Wagner, J. B.; Davies, T. E.; Lu, L.; et al. *Nature* **2016**, *531*, 83−87.
(235) Weckhuysen, B. M. *Phys. Chem. Chem. Phys.* **2003**, *5*, 4351−4360.
(236) Topsøe, H. *J. Catal.* **2003**, *216*, 155−164.
(237) Brown, C.; Krzystek, J.; Achey, R.; Lita, A.; Fu, R.; Meulenberg, R. W.; Polinski, M.; Peek, N.; Wang, Y.; van de Burgt, L. J.; Profeta, S.; Stiegman, A. E.; Scott, S. L. *ACS Catal.* **2015**, *5*, 5574−5583.
(238) Kornienko, N.; Resasco, J.; Becknell, N.; Jiang, C.-M.; Liu, Y.-S.; Nie, K.; Sun, X.; Guo, J.; Leone, S. R.; Yang, P. *J. Am. Chem. Soc.* **2015**, *137*, 7448−7455.
(239) Zhang, S.; Plessow, P. N.; Willis, J. J.; Dai, S.; Xu, M.; Graham, G. W.; Cargnello, M.; Abild-Pedersen, F.; Pan, X. *Nano Lett.* **2016**, *16*, 4528−4534.
(240) Li, P.; Xin, Y.; Li, Q.; Wang, Z.; Zhang, Z.; Zheng, L. *Environ. Sci. Technol.* **2012**, *46*, 9600−9605.
(241) Getsoian, A.; Das, U.; Camacho-Bunquin, J.; Zhang, G.; Gallagher, J. R.; Hu, B.; Cheah, S.; Schaidle, J. A.; Ruddy, D. A.; Hensley, J. E.; et al. *Catal. Sci. Technol.* **2016**, *6*, 6339−6353.
(242) Merle, N.; Le Quéméner, F.; Bouhoute, Y.; Szeto, K. C.; De Mallmann, A.; Barman, S.; Samantaray, M. K.; Delevoye, L.; Gauvin, R. M.; Taoufik, M.; Basset, J.-M. *J. Am. Chem. Soc.* **2017**, *139*, 2144−2147.
(243) Ghuman, K. K.; Hoch, L. B.; Wood, T. E.; Mims, C.; Singh, C. V.; Ozin, G. A. *ACS Catal.* **2016**, *6*, 5764.
(244) Estes, D. P.; Siddiqi, G.; Allouche, F.; Kovtunov, K. V.; Safonova, O. V.; Trigub, A. L.; Koptyug, I. V.; Copéret, C. *J. Am. Chem. Soc.* **2016**, *138*, 14987−14997.
(245) Hu, B.; Getsoian, A.; Schweitzer, N. M.; Das, U.; Kim, H. S.; Niklas, J.; Poluektov, O.; Curtiss, L. A.; Stair, P. C.; Miller, J. T.; Hock, A. S. *J. Catal.* **2015**, *322*, 24−37.
(246) Getsoian, A.; Das, U.; Camacho-Bunquin, J.; Zhang, G.; Gallagher, J. R.; Hu, B.; Cheah, S.; Schaidle, J. A.; Ruddy, D. A.; Hensley, J. E.; Krause, T. R.; et al. *Catal. Sci. Technol.* **2016**, *6*, 6339−6353.

DOI: 10.1021/acscatal.7b01767
ACS Catal. 2017, 7, 7543−7557